OXFORD

Cerebral Cortex, 2023, 1–20
https://doi.org/10.1093/cercor/bhad351
Original Article

Increased functional connectivity between the auditory cortex and the frontoparietal network compensates for impaired visuomotor transformation after early auditory deprivation

Li Song[1], Pengfei Wang[1], Hui Li[1], Peter H. Weiss[2,3], Gereon R. Fink[2,3], Xiaolin Zhou[4], Qi Chen[1,2,*]

[1]Center for Studies of Psychological Application and School of Psychology, South China Normal University, Guangzhou 510631, China,
[2]Cognitive Neuroscience, Institute of Neuroscience and Medicine (INM-3), Research Centre Jülich, Wilhelm-Johnen-Strasse, Jülich 52428, Germany,
[3]Department of Neurology, University Hospital Cologne, Cologne University, Cologne 509737, Germany,
[4]Shanghai Key Laboratory of Mental Health and Psychological Crisis Intervention, School of Psychology and Cognitive Science, East China Normal University, Shanghai 200062, China

*Corresponding author: Center for Studies of Psychological Application and School of Psychology, South China Normal University, Guangzhou 510631, China. Email: qi.chen1@fz-juelich.de

Early auditory deprivation leads to a reorganization of large-scale brain networks involving and extending beyond the auditory system. It has been documented that visuomotor transformation is impaired after early deafness, associated with a hyper-crosstalk between the task-critical frontoparietal network and the default-mode network. However, it remains unknown whether and how the reorganized large-scale brain networks involving the auditory cortex contribute to impaired visuomotor transformation after early deafness. Here, we asked deaf and early hard of hearing participants and normal hearing controls to judge the spatial location of a visual target. Compared with normal hearing controls, the superior temporal gyrus showed significantly increased functional connectivity with the frontoparietal network and the default-mode network in deaf and early hard of hearing participants, specifically during egocentric judgments. However, increased superior temporal gyrus-frontoparietal network and superior temporal gyrus-default-mode network coupling showed antagonistic effects on egocentric judgments. In deaf and early hard of hearing participants, increased superior temporal gyrus-frontoparietal network connectivity was associated with improved egocentric judgments, whereas increased superior temporal gyrus-default-mode network connectivity was associated with deteriorated performance in the egocentric task. Therefore, the data suggest that the auditory cortex exhibits compensatory neuroplasticity (i.e. increased functional connectivity with the task-critical frontoparietal network) to mitigate impaired visuomotor transformation after early auditory deprivation.

Key words: connectomics; deaf and early hard of hearing; modularity; neural plasticity; superior temporal gyrus.

Introduction

The spatial orientation of an object can be represented in either egocentric (i.e. relative to the viewer's body/body effectors) or allocentric (i.e. relative to other external objects) reference frames (Paillard 1991; Blouin et al. 1993; Burgess 2006). The egocentric reference frames are particularly critical for guiding smooth visually guided actions, which requires transforming visuospatial representations of external visual objects into visuomotor representations (Galati et al. 2001; Cohen and Andersen 2002). At the neural level, the dorsal attention network (DAN) is involved in coding the general visuospatial representations underlying both the egocentric and allocentric reference frames (Committeri et al. 2004; Chen et al. 2012, 2014; Gomez et al. 2014), whereas the frontoparietal network (FPN) is specifically involved in body-centered visuomotor transformation during the egocentric task (Galati et al. 2000; Committeri et al. 2004; Neggers et al. 2006; Chen et al. 2012, 2014). The deaf and early hard of hearing (DHH) people exhibited superior haptic orientation processing compared with both normal hearing (NH) signers and nonsigners, i.e. with the effect of sign language controlled for (Van Dijk et al. 2013). Additionally, they made more orientation errors for the crossed posture condition during the crossed-arm temporal order judgment task (Sharp et al. 2018). These findings suggested that early auditory deprivation shifts the balance of reference frames. Since auditory signals interact with the tactile and the motor system during posture, balance, and movement initiation (Queralt et al. 2008; Kanegaonkar et al. 2012; Gandemer et al. 2017), early auditory deprivation might impair these body-related motor processes (Houde et al. 2016; Sharp et al. 2018). Accordingly, previous evidence from our lab shows that processes relying on the egocentric reference frame are impaired after early auditory deprivation (Zhang et al. 2014). The latter is associated with an abnormal hyper-crosstalk between the task-critical FPN and the task-negative default-mode network (DMN) during body-centered egocentric judgments in the DHH individuals (Li et al. 2022).

Early auditory deprivation leads to structural and functional reorganization of the auditory cortex (Amaral and Almeida 2015; Cardin et al. 2020; Hribar et al. 2020; Simon et al. 2020; Yusuf et al. 2021, 2022), which is mainly located in the superior temporal gyrus (STG; Morosan et al. 2001, 2005). Structurally, decreased

Received: April 28, 2023. **Revised:** September 4, 2023. **Accepted:** September 5, 2023

fractional anisotropy of white matter fibers, decreased white matter volume, and increased cortical thickness have been observed in the auditory cortex of DHH people compared with NH controls (Emmorey et al. 2003; Smith et al. 2011; Karns et al. 2016; Kumar and Mishra 2018). However, it remains unknown whether these brain structural changes in the DHH people, such as the increased cortical thickness of the auditory cortex, are associated with impaired visuomotor transformation. Functionally, early auditory deprivation causes cascading neurological and neurocognitive changes (Kronenberger et al. 2014; Kral et al. 2016). Especially, the auditory cortex of the DHH people undergoes cross-modal reorganization and starts to process stimuli from the remaining sensory modalities, such as visual and vibrotactile stimuli (Levänen et al. 1998; Karns et al. 2012; Ding et al. 2015; Bola et al. 2017; Cardin et al. 2018). Furthermore, altered task-evoked or intrinsic functional connectivity between the auditory cortex and other brain regions has been revealed during a variety of cognitive tasks (Shiell et al. 2015; Ding et al. 2016; Benetti et al. 2017, 2021; Bola et al. 2017), indicating large-scale network reorganization in the DHH people. For example, besides the large-scale network reorganization beyond the auditory system (Li et al. 2022), the auditory cortex of the DHH people exhibits stronger intrinsic connections with subregions of the DMN and the FPN compared with NH controls (Ding et al. 2016; Cardin et al. 2018; Andin and Holmer 2022). However, it remains unclear how the decreased network segregation between the "deprived" auditory system, the task-critical DAN and FPN, and the task-negative DMN contributes to the impaired visuomotor transformation after early auditory deprivation. To answer how the structural changes and the large-scale network reorganization involving the auditory cortex are associated with impaired visuomotor transformation in DHH individuals, we reanalyzed the data from a previous fMRI study (Li et al. 2022).

For the network analyses, we focused on the cross-modal reorganization of the functional connectivity between the STG, the task-critical DAN and FPN, and the task-negative DMN in the DHH individuals during an egocentric judgment task. If the task-specific reorganization of a large-scale brain network involving the STG helps compensate for the impaired visuomotor transformation after early auditory deprivation, we expected that: (i) compared with the NH controls, the STG should show enhanced between-module connectivity with the task-critical FPN in the DHH individuals, specifically during the egocentric task and more importantly (ii) the potentially enhanced STG-frontoparietal connectivity should be associated with improved egocentric performance in the DHH people. Moreover, we have previously revealed that impaired visuomotor transformation after early auditory deprivation is associated with abnormal hyper-connectivity between the task-critical frontoparietal regions and the DMN (Li et al. 2022). Therefore, if the STG in the DHH individuals' brain is reorganized to be more integrated, as manifested in increased functional connectivity with the frontoparietal regions during the egocentric task, it may also exhibit increased connectivity with the DMN. Moreover, similar to the increased FPN-DMN connectivity, the potentially increased STG-DMN connectivity should also interfere with the egocentric processing, resulting in a detrimental egocentric performance of DHH people.

In addition, spontaneous neural activity during rest is organized in multiple specific large-scale networks (Damoiseaux et al. 2006; De Luca et al. 2006; Fox and Raichle 2007). These intrinsic brain networks at rest may function as a potential "scaffold" that undergoes subtle reconfigurations to form task-specific generative architectures (Smith et al. 2009; Cole et al. 2014, 2016; Tavor et al. 2016; Pezzulo et al. 2021). The changes in brain network configurations from rest to task states have been shown to predict individuals' task performance (Schultz and Cole 2016; Hearne et al. 2017; Alavash et al. 2019). In the present study, we also tried to investigate whether the DHH participants and the NH controls undergo an adaptive reconfiguration of intrinsic/resting-state large-scale networks during the transition from the resting state to the egocentric task.

Materials and methods

In the current study, we reanalyzed the fMRI data from Li et al. (2022). Li et al. (2022) investigated the reorganization of large-scale brain networks extending beyond the auditory system. In the present study, however, we focused on the reorganization of large-scale brain networks involving the auditory system. Specifically, we investigated whether and how the reorganized connectivity between the auditory system, the DAN, the FPN, and the DMN contributes to the impaired egocentric processing in DHH people. Therefore, we targeted a different research question than Li et al. (2022). Given that the two studies share demographic information about the DHH participants and the NH controls and behavioral results, we will refer this information to Li et al. (2022) when appropriate.

Participants

Please see Li et al. (2022) for detailed demographic information on both subject groups. Briefly, 26 right-handed early DHH individuals (12 males; 21.54 ± 2.06 years old, mean ± SD) and 24 right-handed demographic-matched NH controls (12 males; 21.58 ± 1.69 years old, mean ± SD) participated in this study. Only the DHH and NH participants who reported no subjectively experienced balance problems and no clinical diagnosis of vestibular dysfunction were tested in the present study. All DHH participants had congenital, profound bilateral hearing loss (>90 dB, each ear), as determined by a standard pure-tone audiometry procedure at 500, 1,000, 2,000, and 4,000 Hz. Hearing loss was because of genetic or pregnancy-related factors, like hereditary deafness or drug side effects. The DHH participants exhibited inconsistent speech comprehension, ranging from poor to good, even with hearing aids. Each DHH participant was proficient in Chinese Sign Language but had poor speech articulation. The NH controls were native Chinese speakers who had no prior hearing problems. All participants had normal or corrected-to-normal vision, no color vision impairment, and no psychiatric or neurological diseases. Each participant had signed informed consent following the Helsinki Declaration before the experiment and got paid afterward. The Ethics Committee of the Department of Psychology, South China Normal University, approved this research.

Experimental design

The experimental procedure was controlled using the Presentation software (Neurobehavioral Systems, RRID: SCR_002521, https://www.neurobs.com/). The stimuli consisted of a fork lying on an orange plate displayed on a gray background (Fig. 1A). The luminance of the fork was either dark (RGB: 64, 64, 64) or light (RGB: 192, 192, 192) gray. The width of the fork end was 2.5° of the visual angle, and the diameter of the plate was 15° of the visual angle. The fork was located at four different egocentric positions relative to the midsagittal line of the observer's own body (i.e. −2.67°, −1.7°, 1.7°, and 2.67°) and meanwhile at four different

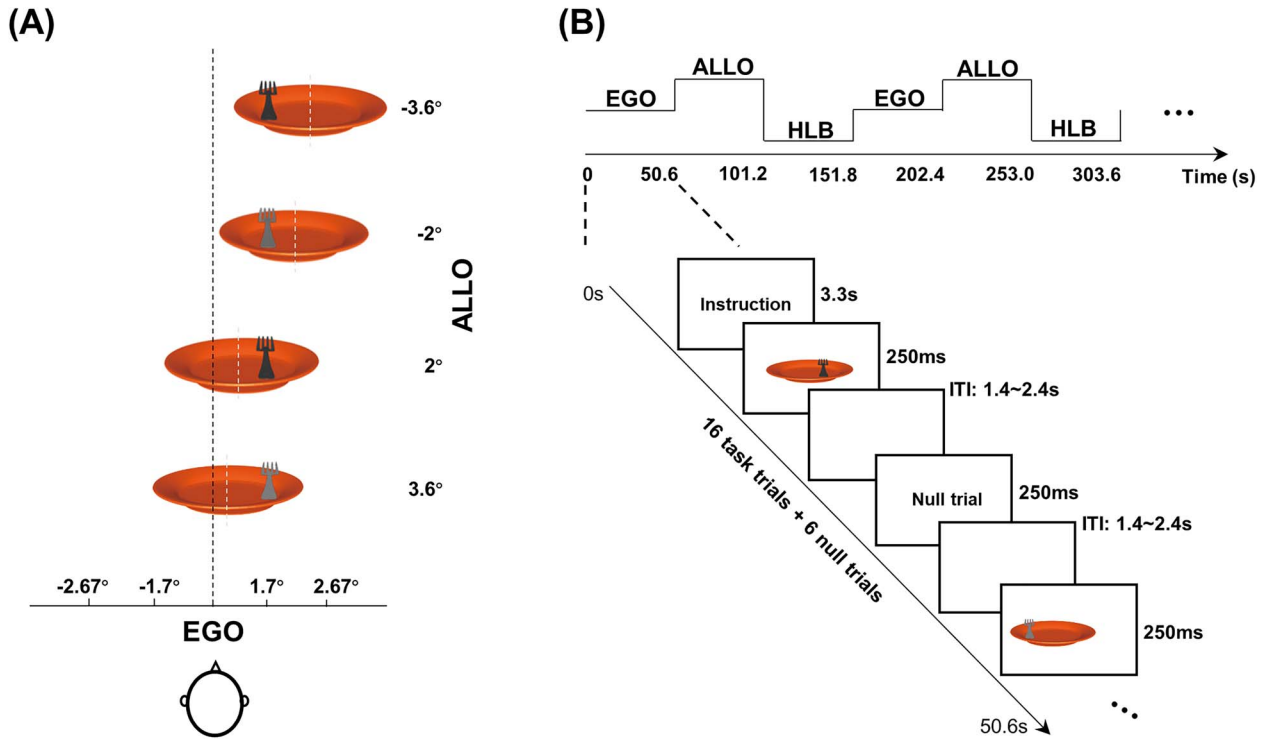

Fig. 1. Stimuli and paradigm (adapted from Li et al. 2022). A) Stimuli. The stimuli consisted of a fork lying on a plate. The luminance of the fork was either dark or light gray. The fork was located at four different egocentric positions (−2.67°, −1.7°, 1.7°, and 2.67°) relative to the midsagittal line of the observer's own body, i.e. the black vertical dashed line. Meanwhile, at each of the four egocentric locations of the fork, the background plate was moved around the fork, forming four different allocentric positions (−3.6°, −2°, 2°, and 3.6°) relative to the midsagittal line of the plate, i.e. the gray vertical dashed line. The egocentric and the allocentric positions were orthogonally crossed. B) Paradigm. A mixed fMRI design was used. Three tasks were presented as alternating task blocks with pseudo-random order, and an event-related design was embedded in each task block. At the beginning of each block, a 3.3 s instruction was displayed to indicate the task of the upcoming block. In the egocentric task (EGO), participants were asked to judge the fork location relative to their bodies' midsagittal plane (left vs. right). In the allocentric task (ALLO), participants were asked to judge the fork location relative to the plate's midsagittal plane (left vs. right). In the HLB task, participants were asked to judge the luminance of the fork (dark vs. light gray). Within each task block, 16 task trials and 6 null trials (only a blank default screen) were randomly mixed with the ITI jittered from 1.4 to 2.4 s in a step of 250 ms. The target in each trial was presented for 250 ms.

allocentric positions relative to the midsagittal line of the plate (i.e. −3.6°, −2°, 2°, and 3.6°). The two types of positions were orthogonally crossed. At each of the four egocentric locations of the fork, the background plate was moved around the fork, forming four different allocentric positions (Fig. 1A). The visual angles of the egocentric and allocentric positions of the targets were set via an initial psychophysical test using a different group of NH individuals to balance the task difficulty between the allocentric and egocentric judgments in the NH controls. Our previous studies demonstrated that these selected allocentric and egocentric positions effectively balanced the task difficulty across the three experimental tasks in the NH participants (Liu, Li, et al. 2017; Li et al. 2022).

All participants performed three different tasks on the same set of stimuli, including the egocentric judgment task (EGO), the allocentric judgment task (ALLO), and the nonspatial luminance discrimination task (i.e. high-level baseline, HLB). In the egocentric task, individuals judged whether the fork was on the left or right side of their bodies' midsagittal plane. In the allocentric task, individuals judged whether the fork was on the left or right side of the plate's midsagittal plane. For these two spatial tasks, participants had to press the left button box with their left thumb for the response of the "left-side" and the right button box with their right thumb for the response of the "right-side." In the nonspatial HLB task, individuals judged the luminance of the fork (dark gray or light gray) by pressing the left button box with their left thumb or the right button box with their right thumb. The mapping between the luminance and response hand was counterbalanced across participants. The experimental design was a 2 (between-subject factor: DHH vs. NH) × 3 (within-subject factor: ALLO, EGO, and HLB) two-factorial design.

In this study, a mixed fMRI design was used. Three types of tasks were presented as alternating task blocks with pseudo-random order, and an event-related design was embedded in each task block (Fig. 1B). All participants alternately performed these three types of tasks 10 times without any rest block. A pseudo-random order rather than a random order of all the task blocks ensured that the maximum time interval between any two identical blocks did not exceed 200 s, thereby meeting the high-pass filter of 1/200 Hz for the following processing of the task-state fMRI data. At the beginning of each block, a 3.3 s instruction was displayed to indicate the task of the upcoming block. Within each task block, 16 task trials and 6 null trials (only a blank default screen) were randomly mixed with the intertrial intervals (ITI) jittered from 1.4 to 2.4 s in 250 ms steps. The target in each trial was presented for 250 ms (Fig. 1B). Such a short stimulus duration was used to minimize eye movements (Findlay 1997). The entire experiment included 160 experimental trials for each type of task and 180 null trials. Notably, no central fixation cross was presented throughout this experiment to avoid participants using it, rather than the task-required body's midsagittal plane, as an allocentric reference object to perform the egocentric task. Participants were also asked to keep their eyes straight ahead and not move their eyeballs. Our previous research using eye-tracking

technology in a comparable experimental paradigm found that central fixation could be maintained equally well in the allocentric and egocentric tasks (Chen et al. 2012). Before the formal fMRI experiment, each participant underwent a training procedure to become familiar with the experimental tasks.

Data acquisition

The imaging data were collected using a SIEMENS 3.0T Trio Tim system with a 32-channel head coil at the Institute of Psychophysics, Chinese Academy of Sciences, Beijing. First, resting-state images were acquired using a T2-weighted EPI sequence with 200 functional volumes. The corresponding parameters as follow: slice thickness = 3 mm, repetition time = 2200 ms, echo time = 30 ms, acquisition matrix = 64 × 64, flip angle = 90°, pixel size = 3.44 × 3.44 × 3.0 mm^3, slices = 36 with a 0.75 mm gap. This resting-state session lasted for 7.33 min. During this session, participants were asked to relax, stay awake with closed eyes, and think about nothing. A T2-weighted EPI sequence with 729 volumes was then used to acquire individual task-state images, and the scanning parameters were the same as the resting-state session. This task-state fMRI scanning had only one run and lasted for 26.73 min. Finally, high-resolution structural images were acquired using a 3D MPRAGE T1-weighted sequence with 144 volumes lasting 8.09 min. The corresponding parameters were: slice thickness = 1.33 mm, repetition time = 2530 ms, echo time = 3.37 ms, inversion time = 1100 ms, acquisition matrix = 256 × 192, flip angle = 7°, pixel size = 0.5 × 0.5 × 1.33 mm^3.

Analysis of structural MRI data

To investigate whether and how the potential structural changes in the brain anatomy of the DHH individuals are associated with egocentric processing, we calculated surface-based cortical thickness for each participant using the CAT12 toolbox (http://www.neuro.uni-jena.de/cat/), which is a well-established pipeline in the SPM12 software (https://www.fil.ion.ucl.ac.uk/spm/software/spm12/) running on MATLAB R2019a. Subsequently, the between-group difference was tested, and the correlation analysis between the cortical thickness and the egocentric performance was performed for each group.

Specifically, individual structural MRI images were corrected for bias field and then segmented into gray matter, white matter, and cerebrospinal fluid. The projection-based thickness method was then used to estimate the cortical thickness (Dahnke et al. 2013), and a 15 mm full-width/half-maximum Gaussian kernel was used to smooth the established central surfaces. An automated quality check and further visual inspection were performed, and all structural images passed through the quality control protocol. The between-group difference in the cortical thickness was tested using the full factorial design via the CAT12. Here, a less conservative threshold with a cluster level of $P < 0.05$ (uncorrected) and a standard voxel level of $P < 0.005$ (uncorrected) was used to identify structural changes in the DHH participants since no group differences were observed at a more conservative threshold of $P < 0.05$, FWE correction for multiple comparisons at the cluster level with a standard voxel level of $P < 0.005$ (uncorrected). Furthermore, we calculated the Pearson correlation between the mean cortical thickness in the anatomical regions with structural alterations and the individual egocentric performance in each group of participants. Because we targeted the specific effect of the egocentric performance rather than the general effect of response speed, the relative reaction time (RT) difference between the egocentric and allocentric tasks ("EGO_RT − ALLO_RT") was used as the behavioral index for the egocentric performance in each participant. In this way, the general response speed in a single participant, which manifests in both the egocentric and allocentric tasks, was canceled out. For demonstration purposes, the thickness values of regions with structural alterations were shown as a function of the two groups, and no further statistical tests were performed to avoid the problem of double-dipping (Kriegeskorte et al. 2009, 2010).

Network nodes definition

Preprocessing of the task-state fMRI data

Task-state fMRI data were preprocessed using SPM12 software. The preprocessing included the following steps: (i) removing the first 5 volumes to ensure the data were collected when the magnetic field was stable and that participants had adapted to the scanning environment, (ii) realigning the functional images to the new first volume to correct head movements, (iii) normalizing all images to standard MNI152 space and resampling voxel size to 3 × 3 × 3 mm^3, and (iv) smoothing with a 6 mm full-width/half-maximum to alleviate the anatomical variability between participants.

Statistical analysis

Preprocessed data were high-pass filtered at 1/200 Hz and modeled with a general linear model (GLM) in SPM12. The temporal autocorrelation was modeled using an AR(1) process. The GLM was used to construct a multiple regression design matrix at the individual-level analysis. Three types of target trials (ALLO, EGO, and HLB) were modeled in an event-related analysis. The three types of neural events were time-locked to the onset of the target trials by a canonical HRF and its first-order time derivative with an event duration of 0 s. Besides, the instructions, the invalid trials (missed, error, and outliers), and the 6 head movement parameters were modeled as another regressor of no interest. The null trials were not modeled and treated as the implicit baseline in the GLM model. Parameter estimates were calculated for each voxel using weighted least squares to provide maximum likelihood estimators based on the temporal autocorrelation of the data. For each participant, simple main effects for the three experimental conditions were computed and taken to a group-level analysis. Specifically, at the group-level analysis, two factors were included in a full factorial model with one task type factor (ALLO, EGO, and HLB) and one group factor (DHH vs. NH). To test whether the cross-modal reorganization occurred in the auditory system of the DHH participants' brains, a t-test contrast of "DHH (ALLO + EGO + HLB) > NH (ALLO + EGO + HLB)," collapsed over all three visual tasks, was established. In this way, the reorganized regions that displayed significantly elevated neural activity during the three visual tasks in the DHH than the NH group were included. To further test whether the neural interactions between the auditory cortex and the task-related regions were altered in the DHH participants' brains, an F-test contrast of "the main effect of tasks," i.e. "ALLO vs. EGO vs. HLB," collapsed over the two groups, was established. In this way, the brain regions that showed differential (positive and negative) activation between the three tasks were included. Areas of activation were identified as significant if they passed a threshold of $P < 0.005$, FWE correction for multiple comparisons at the cluster level with an underlying voxel level of $P < 0.001$ (uncorrected). The localized task-related regions, together with the reorganized auditory cortex, were combined to form a brain mask, and each voxel of this mask was considered a node in the subsequent modularity analyses. For demonstration purposes, mean parameter estimates were extracted from the reorganized clusters and displayed as a function of the two

groups. No extra statistical tests were additionally performed on the extracted parameter estimates.

Modularity analyses

Data preprocessing

Resting-state fMRI data were preprocessed using the DPARSF module of the DPABI V6.0 software (http://rfmri.org/DPABI). The preprocessing included the following steps: (i) discarding the first 5 volumes, (ii) slice timing correction, (iii) head movement correction, (iv) reorienting functional and structural images to achieve high-quality segmentation and normalization, (v) controlling for Friston-24 motion parameters, white matter signal, and cerebrospinal fluid signal as covariates, (vi) normalizing functional images to standard MNI152 space using DARTEL and resampling voxel size to $3 \times 3 \times 3$ mm^3, and (vii) bandpass filtering with 0.01–0.1 Hz. Given that removing the global signal would change the distribution of connectivity and increase negative correlations (Murphy et al. 2009; Liu, Nalci, et al. 2017; Murphy and Fox 2017), the global signal was not regressed out. The network node was each voxel in our predefined task mask. Hence, spatial smoothing, which would exaggerate the similarity between voxels, was not performed. The same preprocessing of the resting-state fMRI data was also applied to the task-state fMRI data to minimize the impact of preprocessing differences and ensure the comparability of modularity results between the resting-state and the task-state.

Network construction

For the resting-state data, we extracted the whole time series of each voxel from our task mask and calculated the voxel-wise Pearson correlation matrix on the individual level, which was used to represent the edges of graph analysis. Notably, the task mask was used in the resting-state graph analysis to ensure that the same nodes were included as in the task-state graph analysis. For the task-state data, blocks with more than 6 error trials were discarded. Accordingly, 4 of the 26 DHH participants and 4 of the 24 NH controls had removed task blocks. Specifically, for the DHH group, 1 ALLO block and 1 EGO block were discarded in one participant, and 1 EGO block was discarded in the other three participants. For the NH group, 1 ALLO block and 1 HLB block were discarded in two participants, 1 EGO block was discarded in one participant, and 1 HLB block was discarded in one participant. There were 16 experimental trials in each task block. Therefore, for the DHH group, 4 EGO blocks (i.e. 4*16 = 64 EGO trials, 1.54%) in total and 1 ALLO block (i.e. 16 ALLO trials, 0.38%) in total were discarded across all the DHH participants. For the NH group, 1 EGO block (i.e. 16 EGO trials, 0.42%) in total, 2 ALLO blocks (i.e. 2*16 = 32 ALLO trials, 0.83%) in total, and 3 HLB blocks (i.e. 3*16 = 48 HLB trials, 1.25%) in total were discarded across all the NH participants. Given the effect of hemodynamic delay, the first 4 volumes (8.8 s) were removed, and the 2 volumes (4.4 s) of the next block were included in each valid block (Mostofsky et al. 2009), so there were 20 time points per block. The time series of each voxel from our mask was extracted, and a voxel-wise Pearson correlation matrix was calculated within each valid block on the individual level. All correlation matrices for each participant's task were then averaged (Mostofsky et al. 2009; Liang et al. 2016), resulting in one correlation matrix for each task type in each participant. A set of sparsity thresholds (2–5% with a step of 1%, i.e. the ratio of the number of actual edges to the maximum possible number of edges) was selected to ensure the sparsity nature of the brain network and simultaneously remove weak correlations. Subsequently, edges in binary networks were defined by assigning the value of 1 to the connections that survived a given threshold and 0 to the other connections. Because of the controversial physiological meaning of the negative connections (Anderson et al. 2011; Schwarz and McGonigle 2011; Keller et al. 2013), negative correlations were assigned the value 0 and removed from further analyses (Liang et al. 2016; Sun et al. 2017; Sha et al. 2018; Guo et al. 2019; Sulpizio et al. 2020). Therefore, we focused on the positive connections in our analyses by setting the negative correlations to 0.

Evaluating network properties

The graph-based modularity analyses were conducted on the resultant brain graphs via the GRETNA V2.0 software (https://www.nitrc.org/projects/gretna/). In order to identify brain modules, sets of nodes that are highly associated with each other but less associated with other modular nodes, the modified greedy optimization algorithm (Fortunato 2010) was used in which the modularity (Q) was defined as:

$$Q = \sum_{s=1}^{N_M} \left[l_s/L - \left(d_s/2L \right)^2 \right],$$

where N_M is the number of nonoverlapping modules, l_s is the number of within-module links in the module s, L is the total number of links in the network, d_s is the sum of degrees for each node in the module s, and the degree is the number of links connected to a node (Guimerà and Amaral 2005). The modularity of a given network quantifies the extent to which the network can be subdivided into modules with higher within-module than between-module connections (Newman and Girvan 2004). In real-world networks, modularity typically falls in the range of 0.3–0.7 (Newman and Girvan 2004).

We first performed the individual-level modularity analysis based on each participant's brain graph for the resting-state fMRI data. Since the module number and membership varied among individuals even within the same group, a group-level modularity analysis (collapsed over the two groups) was also performed to obtain a general modular structure shared by all the participants. Specifically, a group brain graph was created by averaging the correlation matrices across all participants and then thresholding at each network sparsity threshold from 2% to 5% in a step of 1%. After the group-level modularity analysis, the adjusted mutual information (AMI) was estimated to measure the similarity of module structure between the two groups. Since the modular partitions were similar between the DHH and NH groups based on the AMI analysis (see Results), the modules of interest comprising the DAN, the FPN, the DMN, and the bilateral STG were selected from the group-level modularity analysis at the moderate network sparsity of 3%. The sparsity of 3% was chosen based on the quality of the module partition (Liang et al. 2016). The present study was specially designed to explore the functional connectivity between the auditory system, the DAN, the FPN, and the DMN. Therefore, precise and reasonable identification of the four modules is the rule of thumb for sparsity selection in the present study. Although the step size of sparsity change is only 1%, there are significantly various module partitions at the different sparsity thresholds. For example, the number of edges included in module identification between each 1% step is very different, i.e. 9,830*(9,830 − 1)/2*1%, where 9,830 is the number of nodes in our study (Rubinov and Sporns 2010). Low sparsity levels will generate disconnected graphs where the networks become severely fragmented (Meunier et al. 2009; Power et al. 2011). In our case, at the sparsity of 2% (see Results), the DMN

was divided into three separate modules, and the FPN was divided into two separate modules. On the other hand, higher sparsity levels will generate graphs with low modularity equivalent to a random graph where the different networks are merged into one module (Meunier et al. 2009; Power et al. 2011). In our case, at the sparsity of 4% and 5% (see Results), the auditory cortex and part/all of the DAN were identified as one single module, and the bilateral insular regions were merged with the FPN. Because of the inaccurate network partitions at the sparsity of 2%, 4%, and 5%, it was challenging to answer, for example, how the connectivity between the auditory system and the DAN was reorganized in the DHH brain when the two modules were fragmented into several sub-modules (at the sparsity of 2%) or when the two modules were (partly) mixed (at the sparsity of 4% and 5%). Thus, we did not conduct further analyses at the sparsity thresholds of 2%, 4%, and 5%. This approach follows most previous studies adopting graph theory analyses: only the sparsity level with the most precise and reasonable network partition was selected and entered into further analyses (e.g. Meunier et al. 2009; Gratton et al. 2012; Liang et al. 2016; Gordon et al. 2017; Sun et al. 2017; Yoo et al. 2019; Liu et al. 2020; Ma et al. 2020; Lei et al. 2022). Among the segmented modules at the sparsity of 3%, the DAN, the FPN, and the DMN modules were visually identified according to the Yeo-7 networks (Yeo et al. 2011), and the STG was visually identified based on the Automated Anatomical Labeling template (Tzourio-Mazoyer et al. 2002). Based on the above identified modules, the network properties at the nodal and the modular levels were then calculated during the resting and the task state, respectively.

In this study, we focused on the reorganization of the between-module connectivity involving the STG in the DHH individuals. Accordingly, the participation coefficient (PC) across the four modules of interest (DMN, DAN, FPN, and STG) was calculated at the nodal level. Since we were interested in the alterations of the inter-module connectivity between the STG and each of the three task-related networks (DAN, FPN, and DMN), the PC was estimated only between any pair of two modules involving the STG. The PC reflects the ability of a node i to keep communication between its own module and the other modules, defined as:

$$PC_i = 1 - \sum_{s=1}^{N_M} \left(\frac{k_{is}}{k_i} \right)^2,$$

where N_M is the number of nonoverlapping modules (i.e. "2" for the current analysis), k_{is} is the number of positive links between node i and module s, and k_i is the sum number of positive links of node i in the network (including two modules in the current analysis; Guimerà and Amaral 2005). Therefore, if the links of node i are distributed across all modules, the node's PC is close to 1, and if the links of node i are within its corresponding module, the node's PC is close to 0.

At the modular level, we also calculated the between-module connectivity (STG-DAN, STG-FPN, and STG-DMN) for each participant during both the resting state and the egocentric task by averaging the PC values across all nodes/voxels in the two modules belonging to the same pair of modules (Geerligs et al. 2015; Sadaghiani et al. 2015; Baum et al. 2017).

Statistical analysis

For the node-wise analysis, the PC image file for each participant was created based on individual nodes' PC values, and the created images were then submitted to a group-level analysis in SPM12. More specifically, the two-sample t-test was implemented for the resting-state data, whereas the full factorial model with one task type factor (ALLO, EGO, and HLB) and one group factor (DHH vs. NH) was implemented for the task-state data. During the task-state modularity analyses, we were particularly interested in the altered inter-module connectivity between the STG and the task-related networks, specifically during the egocentric task in the DHH participants compared with the NH controls. Therefore, an exclusive masking procedure was performed to eliminate the potential contribution from the other task of no interest, i.e. the contrast "DHH EGO > NH EGO" was exclusively masked by the contrast "DHH ALLO > NH ALLO." More concretely, a mask was first built based on the contrast "DHH ALLO > NH ALLO" at a liberal threshold of uncorrected voxel level of $P < 0.05$. Then, we discarded those significant voxels in this mask from the brain activations related to the target contrast "DHH EGO > NH EGO." In this way, the voxels that showed an altered neural coupling during the allocentric task in the DHH group when compared with the NH group ($P < 0.05$, uncorrected at the voxel level) were excluded from the analysis, leaving the specific alteration of neural coupling during the egocentric task in the DHH participants. To investigate whether and how the inter-module connections would benefit or harm the egocentric processing, we built a new model with only the egocentric PC images for both groups of participants and with their egocentric performance ("EGO_RT – ALLO_RT") as a covariate. Areas of activation were identified as significant if they passed a threshold of $P < 0.05$, FWE correction for multiple comparisons at the cluster level with an underlying voxel level of $P < 0.05$ (uncorrected). For demonstration purposes, mean PC values were extracted from the significantly activated regions and shown as a function of the subject group. No further statistical tests were performed to avoid double-dipping. Behavior-related activation did not survive correction for multiple comparisons, but several meaningful subthreshold results merited further exploration. As such, an uncorrected threshold of $P < 0.05$ was used to identify a trend toward significant activation.

For the module-wise analyses, we aimed to investigate whether and how the modular reconfigurations (STG-DAN, STG-FPN, and STG-DMN) occurred in the DHH participants and the NH controls from the resting state to the egocentric task. Within each subject group, paired t-tests, with Bonferroni correction, were adopted to test the difference in the module-level mean PC between the resting state and the egocentric task. Since we already statistically tested the between-group difference at the nodal level, to avoid double-dipping, we did not use a 2 (between-subject factor: DHH vs. NH) × 2 (with-subject factor: Rest vs. EGO) ANOVA, which incorporates the statistical tests of the between-group difference. Finally, to test whether the modular reconfigurations, from the rest to the egocentric task, were associated with the specific effect of individuals' egocentric performance, we calculated the correlation between the between-state changes in the module-level mean PC ("Rest – EGO") and the relative RTs of the egocentric task ("EGO_RT – ALLO_RT").

Results

Structural alternations in the DHH individuals' brain

Surface-based morphometry analyses showed increased cortical thickness in the left STG of the DHH individuals compared with the NH controls (Fig. 2A and Table 1A). Interestingly, a marginally significant correlation between the mean cortical thickness in the left STG and the individual egocentric performance was observed

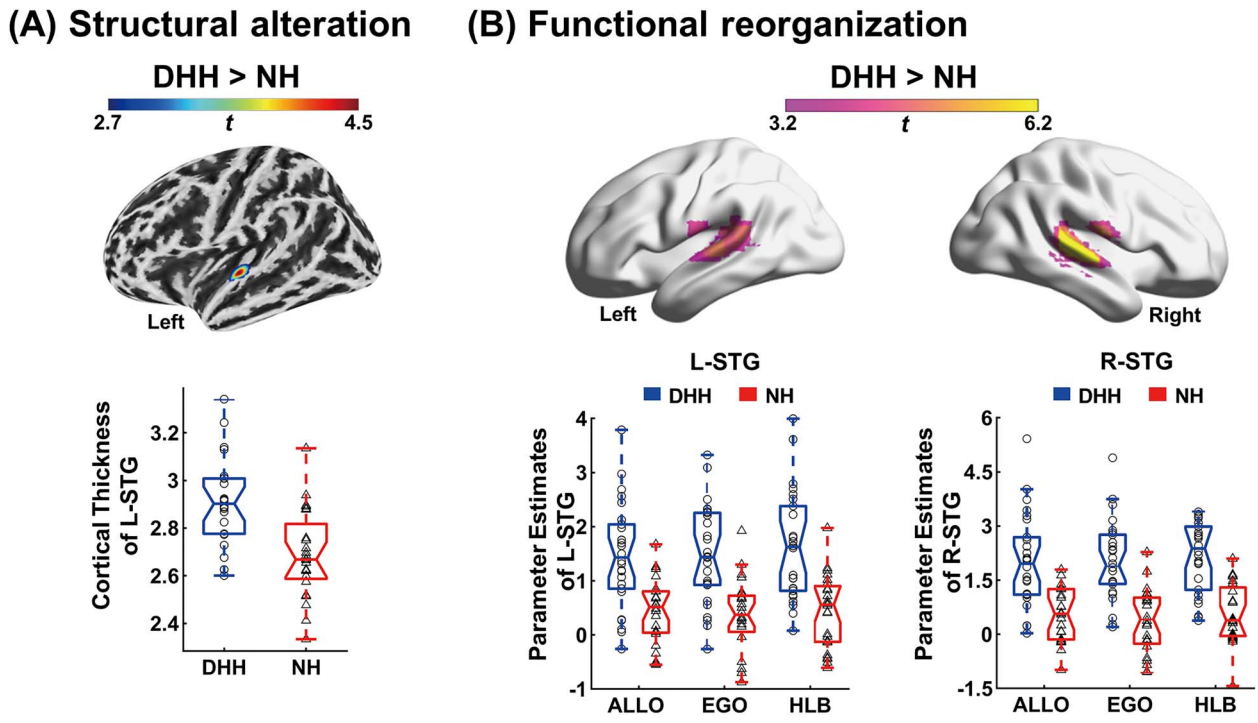

Fig. 2. Structural alteration and functional reorganization in the brains of DHH participants. A) Structural alteration. The DHH group showed increased cortical thickness in the left STG compared with the NH controls. The box plot shows the mean thickness values in the area of structural change for each group. B) Functional reorganization. Compared with the NH controls, the DHH participants showed significantly elevated neural activity in bilateral STG in all three visual tasks (ALLO, EGO, and HLB). The box plots show the mean amplitude of BOLD responses in each group's significantly activated regions in the three tasks. Note that all the box plots are shown only for demonstration purposes, and no further statistical tests were performed to avoid double-dipping. ALLO, allocentric task; EGO, egocentric task; L, left; R, right.

Table 1. Structural alteration and functional reorganization in the STG of the DHH.

Region	Hemisphere	Peak MNI coordinate (mm)	*t*-value	Ke (voxels)
(A) Structural alteration				
Superior temporal gyrus (STG)	L	−54, −14, 4	4.57	143
(B) Functional reorganization				
Superior temporal gyrus (STG)	R	63, −15, 3	6.67	379
	L	−42, −36, 12	5.47	265

DHH, deaf and early hard of hearing; L, left; R, right.

in the DHH participants, $r = 0.38$, $P = 0.056$, i.e. there was a significant trend that the thicker the left STG in a DHH individual, the slower her/his egocentric judgment (Supplementary Fig. 1). However, no significant correlation between the two factors was found in the NH participants ($r = 0.01$, $P = 0.956$).

Cross-modal responses to all the visual tasks in bilateral STG of the DHH individuals' brain

The bilateral STG was significantly activated in the neural contrast "DHH (ALLO + EGO + HLB) > NH (ALLO + EGO + HLB)," indicating that neural activity in the bilateral STG of the DHH participants' brains generally increased upon performing the current three visual tasks, compared with the NH controls (Fig. 2B and Table 1B).

Brain module identification

Via an *F*-test on the task-state fMRI data, we first localized the task-related brain network involved in the differential (positive and negative) activation between any two of the three visual tasks, collapsed over the two groups. An extensive brain network was thus localized, including the DAN, the FPN, and the task-negative DMN (Fig. 3A). Subsequently, the localized task-related network, together with the bilateral STG activated by the three visual tasks in the DHH individuals (see Fig. 2B), was combined as a brain mask image for the subsequent modularity analyses on the resting-state fMRI data.

Results of the modularity analyses on the resting-state data showed high modularity Q values across all the sparsity levels, either in each participant group or in all participants combined (all more than 0.3; Fig. 3B), indicating that the modular structure was a nonrandom community (Newman and Girvan 2004). At each network sparsity threshold, the AMI (DHH vs. NH) ranged from 0.61 to 0.77, suggesting that the modular structure was stable and similar between the two groups (Vinh et al. 2010). The four modules of interest (STG, DAN, FPN, and DMN) could be reasonably identified for both groups at the 2% sparsity threshold (Supplementary Fig. 2A), and the modular partitions, particularly the four modules of interest, were the most similar between the two groups at the sparsity threshold of 2%, through both visual inspection and the value of similarity index—AMI (0.77). At the other three sparsity thresholds (3%, 4%, and 5%), the AMI values were 0.71, 0.61, and 0.71, respectively. However, there were easily noticeable differences in the STG and the DAN modules between the two groups at the disparity thresholds of 3–5%

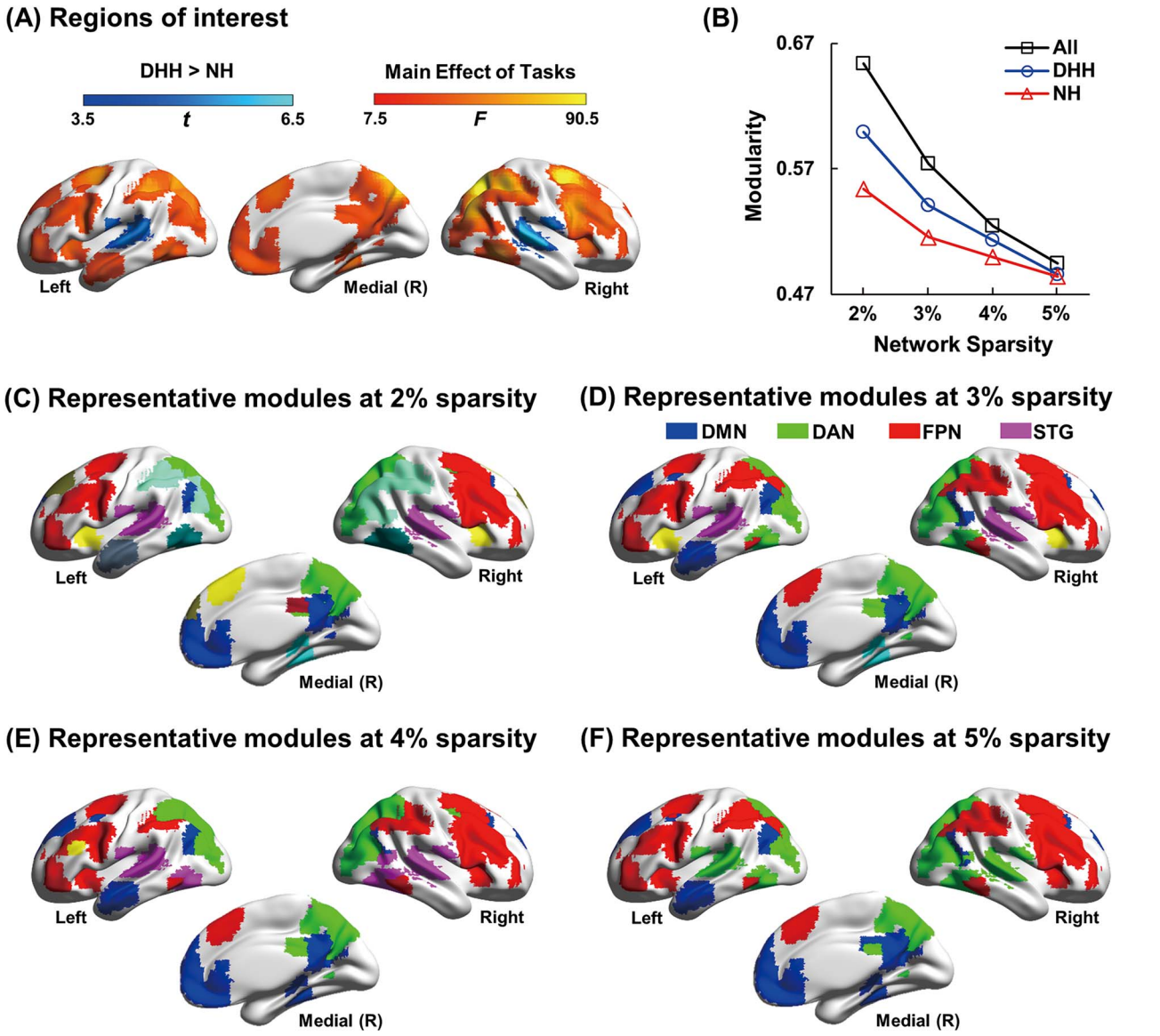

Fig. 3. Module identification. A) The brain mask used for module identification. The regions in warm colors are the brain regions that showed differential (positive or negative) activation between any two of the three tasks "ALLO vs. EGO vs. HLB" for both groups of participants. The regions in cold colors are the bilateral STG that showed significantly elevated neural activity during the three visual tasks in the DHH compared with the NH group, i.e. "DHH (EGO + ALLO + HLB) > NH (EGO + ALLO + HLB)." B) Mean modularity was obtained for the DHH group, the NH group, and all the participants (collapsed over the two groups), respectively, with the network sparsity from 2% to 5% based on the resting-state fMRI data. Maps of representative modules from the resting-state data of all participants at the sparsity thresholds of C) 2%, D) 3%, E) 4%, and F) 5% were shown, respectively. At the network sparsity of 3%, the DMN, the DAN, the FPN, and the STG were well separated. ALLO, allocentric task; EGO, egocentric task; R, right.

(Supplementary Fig. 2B–D). Although the four modules of interest were very similar between the two groups and were well separated at the sparsity of 2% (Supplementary Fig. 2A), they were not 100% identical between the two groups. For example, the bilateral insular regions were merged into the FPN in the NH group, which was not the case in the DHH group (see lateral yellow regions in Supplementary Fig. 2A). Because of the between-group difference in the nodes and edges of the modular partitions, one cannot use the specific modular partitions within the two groups to explore the between-group differences in the inter-module connectivity. Considering the imperative use of identical modules for a fair comparison of inter-module connectivity between the two groups, we adopted the module partitions based on the group-level brain graph (collapsed over the two groups) to obtain a common modular structure. The results showed that the low sparsity threshold at 2% generated a disconnected graph, where the DMN and the FPN became fragmented (Fig. 3C). Rather, the modular partitions were precise and reasonable at the moderate sparsity threshold of 3% (Fig. 3D). The higher sparsity thresholds at 4% and 5% generated graphs with low modularity equivalent to a random graph, where the STG and part/all of the DAN were merged into one single module (Fig. 3E and F). These findings are consistent with previous evidence (Meunier et al. 2009; Power et al. 2011).

Taken together, the modules identified explicitly within each group were most similar between the two groups and most reasonably separated at the sparsity of 2% (Supplementary Fig. 2A), whereas the modules identified across all the participants from both groups were precise and reasonable at the sparsity of 3% (Fig. 3D). This phenomenon mainly results from the different sample sizes in the two analyses: the within-group analyses are based on smaller sample sizes (around 20) than the analysis for both groups combined (over 40). When the number of participants

is smaller, connections with low values in the average functional connectivity matrix are more likely to be spurious connectivity, potentially arising as a mere by-product of the noise in neural data (van Wijk et al. 2010; Fornito et al. 2012; van Den Heuvel and Fornito 2014; van den Heuvel et al. 2017). Therefore, a more stringent sparsity threshold (2% in the present study) was necessary to identify the high and real brain connections and remove the noisy connections to identify accurate modular structures within each group of participants. In contrast, the average correlation matrix obtained from a larger number of participants can mitigate the potentially noisy connections (Roberts et al. 2017; Betzel et al. 2019). Moreover, a larger sample size enables connectivity detection with more precision and reliability (Helwegen et al. 2023). Accordingly, a moderate sparsity threshold (3% in the present study) and more valid connections were sufficient to detect the accurate modular structure when the two groups of participants were combined. Therefore, the module partitions based on the group-level brain graph (collapsed over both groups of participants) were selected at the moderate network sparsity of 3% for further analyses (Fig. 3D). Specifically, 10 modules in total were identified for all participants, and 4 of them (STG, DAN, FPN, and DMN) were selected for the subsequent graph-based analyses on both the resting-state and the task-state data.

Please note that common networks of interest (STG, DAN, FPN, and DMN) between the two groups were also derived via conjunctions between the modular partitions at the same sparsity threshold of 2% within each subject group (Supplementary Fig. 3A). The overlapped networks of interest between the two groups were then used to carry out the validation modular analyses to test the reliability of our findings further. The validation analysis replicated the major results based on the group-level (collapsed across both groups) masks. Please see the Supplementary Material for more information.

The resting state: increased module connectivity between the STG, the DAN, and the FPN in the brain of DHH individuals

For the resting-state data, the between-group difference in the pair-wise connectivity between the STG and the three task-related networks (the DAN, the FPN, and the DMN) was calculated at the nodal level.

Stronger inter-module connectivity between the STG and the DAN was observed in the DHH compared with the NH group (Fig. 4A). Specifically, the right middle occipital gyrus (MOG) extending to the bilateral superior parietal lobe (SPL) and the precuneus within the DAN exhibited significantly higher PC values with the bilateral STG in the DHH than NH group (Fig. 4A, left panel; and Table 2A). Moreover, the bilateral STG exhibited significantly higher PC values with the DAN in the DHH than the NH group (Fig. 4A, right panel; and Table 2A). Besides the DAN, the right inferior frontal gyrus (IFG) in the FPN showed significantly higher PC values with the STG in the DHH than the NH group (Fig. 4B and Table 2B). Taken together, the STG of the DHH showed increased connectivity with subregions both in the DAN and the FPN during the resting state.

The task state: enhanced module connectivity between the STG and the task-related networks during the egocentric task in the brain of DHH individuals

For the task-state data, at the nodal levels, we aimed to investigate the between-group difference (DHH vs. NH) in the inter-module connectivity between the STG and the task-related networks (i.e. DAN, FPN, and DMN), especially during the egocentric task.

Compared with the NH group, we found enhanced connectivity between the STG and subregions of the DAN in the DHH group, specifically during the egocentric task (Fig. 5). More concretely, within the DAN, the right MOG extending into the precuneus showed significantly higher PC values with the STG in the DHH group compared with the NH group, especially during the egocentric task, rather than the allocentric task (Fig. 5A, the left panel; and Table 3A). Moreover, results from the behavior-related model showed that the PC value from the right MOG to the STG was significantly negatively correlated with the individual egocentric performance only in the DHH group but not in the NH group: the stronger the right MOG-STG connectivity in a DHH individual, the faster her/his egocentric judgment (Fig. 5A, the right panel). On the other hand, the right STG also showed significantly larger PC values with the DAN in the DHH than the NH group, especially in the egocentric task, rather than the allocentric task (Fig. 5B and Table 3A).

Besides the DAN, enhanced inter-module connectivity between the STG and the FPN, specifically during the egocentric task, was also found in the DHH rather than the NH group (Fig. 6). The right middle frontal gyrus (MFG), right inferior parietal lobe (IPL), and right superior frontal gyrus (SFG) within the FPN exhibited significantly stronger PC values with the STG in the DHH than NH group especially in the egocentric task, rather than the allocentric task (Fig. 6A, the left panel; and Table 3B). Moreover, results from the behavior-related model showed that the PC value from the right MFG to the STG was significantly negatively correlated with the individual difference in the egocentric performance only in the DHH group but not in the NH group: the stronger the right MFG-STG connectivity in a DHH individual, the faster her/his egocentric judgment (Fig. 6A, the right panel). On the other hand, the PC values from the bilateral STG to the FPN were also significantly higher in the DHH than the NH group, specifically during the egocentric task, rather than the allocentric task (Fig. 6B and Table 3B).

The task state: enhanced module connectivity between the STG and the DMN during the egocentric task in the DHH individuals' brain

For the inter-module connectivity between the STG and the DMN, the neural coupling was significantly higher in the DHH than the NH group, only during the egocentric rather than allocentric task (Fig. 7). Specifically, the medial prefrontal cortex (mPFC) and the posterior cingulate cortex (PCC) in the DMN exhibited significantly larger PC values with the STG in the DHH than the NH group, especially during the egocentric rather than allocentric task (Fig. 7A, the left panel; and Table 3C). Interestingly, results from the behavior-related model showed that the PC value from the PCC to the STG was significantly positively correlated with the individual difference in the egocentric performance only in the DHH group, but not in the NH group: the stronger the PCC-STG connectivity in a DHH individual, the slower her/his egocentric judgment (Fig. 7A, the right panel). On the other hand, the right STG also showed significantly larger PC values with the DMN in the DHH than the NH group during the egocentric rather than allocentric task (Fig. 7B and Table 3C).

Lack of flexibility in network reconfiguration from rest to egocentric task in the brain of DHH individuals

For the inter-module connectivity between the STG and the FPN, the NH controls showed a significant decrease when the brain state transitioned from the rest to the egocentric task, $t = 4.91$, $P < 0.001$ (Fig. 8A, right). The DHH group, however, did

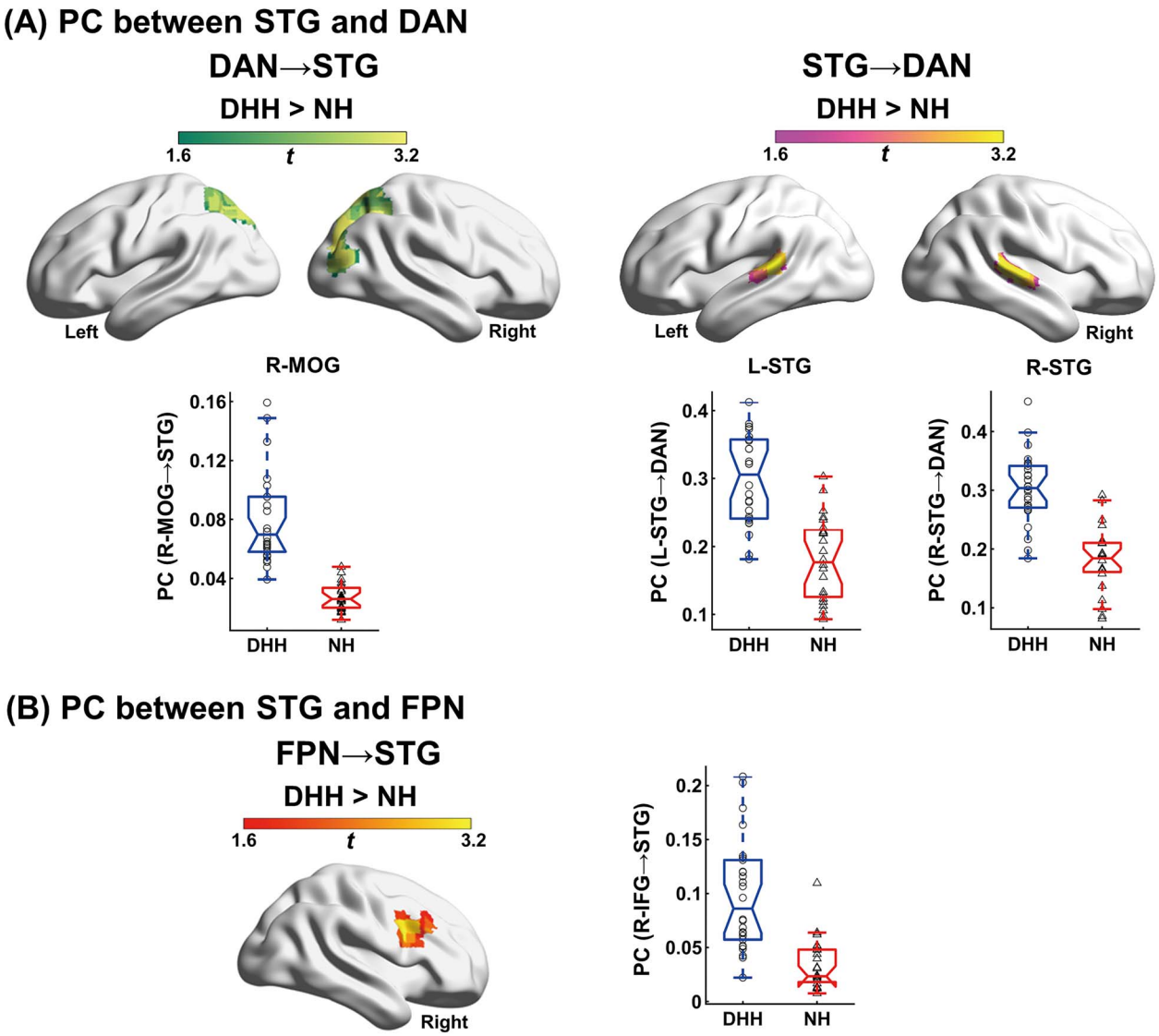

Fig. 4. Resting-state results of module connectivity between the STG, the DAN, and the FPN. A) PC between the STG and the DAN. Left panel: the right MOG extending to the bilateral SPL and the precuneus within the DAN exhibited significantly higher PC values with the STG in the DHH than the NH group during the resting state. Right panel: the bilateral STG exhibited significantly higher PC values with the DAN in the DHH than the NH group during the resting state. B) The right IFG in the FPN exhibited significantly higher PC values with the STG in the DHH than the NH group during the resting state. For demonstration purposes, mean PC values were extracted from the significantly activated regions and shown as a function of the subject group. No further statistical analysis was performed on the extracted PC values to avoid double-dipping. L, left; R, right.

Table 2. Participation coefficient (PC) results between the STG, the DAN, and the FPN during the resting state.

Region	Hemisphere	Peak MNI coordinate (mm)	t-value	Ke (voxels)
(A) PC between STG and DAN				
DAN→STG (DHH > NH)				
Middle occipital gyrus (MOG)	R	30, −78, 24	4.81	449
Precuneus	R	21, −63, 24	4.12	
Cuneus	L	−12, −75, 39	3.93	
Superior parietal lobe (SPL)	R	21, −60, 69	3.73	
STG→DAN (DHH > NH)				
Superior temporal gyrus (STG)	R	57, −24, 9	5.03	60
	L	−54, −30, 9	3.50	42
(B) PC between STG and FPN				
FPN→STG (DHH > NH)				
Inferior frontal gyrus (IFG)	R	51, 15, 30	3.28	80

Italics indicate the coordinates of relevant local maxima within each significant cluster. DAN, dorsal attention network; FPN, frontoparietal network; DHH, deaf and early hard of hearing; NH, normal hearing; L, left; R, right.

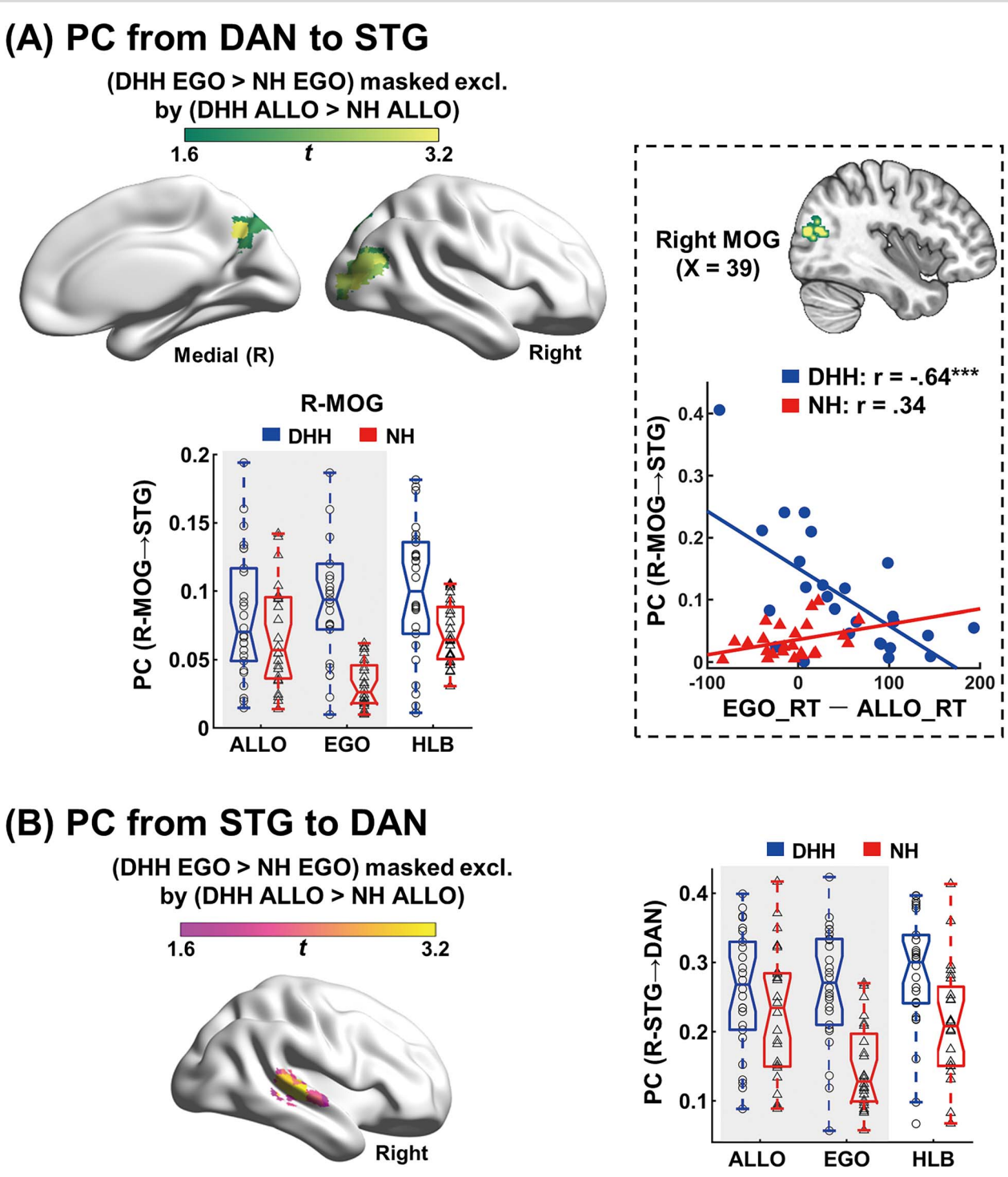

Fig. 5. Task-state PC results between the STG and the DAN. A) PC from the DAN to the STG. Left panel: The interaction effect between the subject group (DHH vs. NH) and the visual tasks (EGO vs. ALLO). The right MOG extending to the precuneus within the DAN exhibited significantly higher PC values with the STG in the DHH than the NH group, especially during the egocentric task rather than the allocentric task. Moreover, the PC value from the right MOG in the DAN to the STG was significantly negatively correlated with the egocentric performance ("EGO_RT – ALLO_RT") only in the DHH group but not in the NH group (right panel). The stronger the right MOG-STG connectivity in a DHH individual, the faster the egocentric judgment. ***$P < 0.001$. B) PC from the STG to the DAN. The right STG showed significantly larger PC values with the DAN in the DHH than the NH group, especially during the egocentric rather than the allocentric task. For demonstration purposes, mean PC values were extracted from the significantly activated regions and shown as a function of the subject group. No further statistical analysis was performed on the extracted PC values to avoid double-dipping. The conditions involved in the neural contrast were shaded. ALLO, allocentric task; EGO, egocentric task; L, left; R, right.

not show such network reconfiguration, $t = 1.07$, $P = 0.30$ (Fig. 8A, left). For both the STG-DAN (Fig. 8B) and the STG-DMN (Fig. 8C) pairs, the inter-module connectivity was comparable between the resting state and the egocentric task in both the DHH group and the NH controls, all $Ps > 0.1$. Besides, no significant correlation was found between the modular reconfiguration and the individuals' egocentric performance in either group, all $Ps > 0.1$.

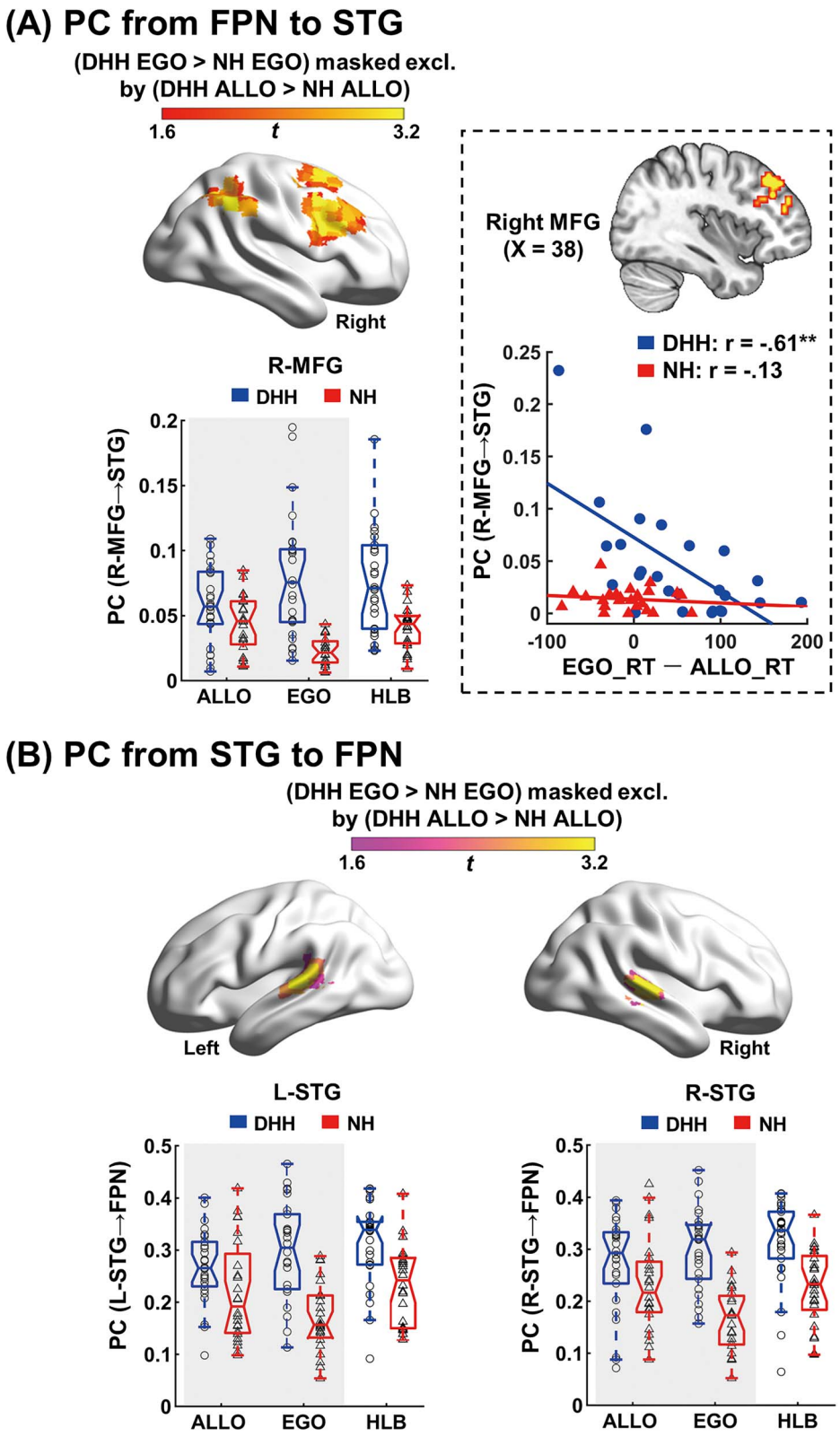

Fig. 6. Task-state PC results between the STG and the FPN. A) PC from the FPN to the STG. Left panel: the interaction effect between the subject group (DHH vs. NH) and the visual tasks (EGO vs. ALLO). Extensive areas in the FPN, including the right MFG, right IPL, and right SFG, exhibited significantly stronger PC values with the STG in the DHH than the NH group, especially during the egocentric rather than the allocentric task. Moreover, the PC value from the right MFG in the FPN to the STG was significantly negatively correlated with the egocentric performance ("EGO_RT – ALLO_RT") only in the DHH group but not in the NH group (right panel). The stronger the right MFG-STG connectivity in a DHH individual, the faster the egocentric judgment. $^{**}P < 0.01$. B) PC from the STG to the FPN. The bilateral STG showed significantly larger PC values with the FPN in the DHH than the NH group, especially during the egocentric rather than the allocentric task. For demonstration purposes, mean PC values were extracted from the representative significantly activated regions and shown as a function of the three tasks in each subject group. No further statistical analysis was performed on the extracted PC values to avoid double-dipping. The conditions involved in the neural contrast were shaded. ALLO, allocentric task; EGO, egocentric task; L, left; R, right.

Table 3. Participation coefficient (PC) results between the STG, the DAN, the FPN, and the DMN during the task state.

Region	Hemisphere	Peak MNI coordinate (mm)	*t*-Value	Ke (voxels)
(A) PC between STG and DAN				
DAN→STG				
(DHH EGO > NH EGO) exclusively masked by (DHH ALLO > NH ALLO)				
Precuneus	R	9, −63, 39	3.40	96
Middle occipital gyrus (MOG)	*R*	*33, −72, 15*	3.15	
STG→DAN				
(DHH EGO > NH EGO) exclusively masked by (DHH ALLO > NH ALLO)				
Superior temporal gyrus (STG)	R	51, −27, 6	3.38	50
(B) PC between STG and FPN				
FPN→STG				
(DHH EGO > NH EGO) exclusively masked by (DHH ALLO > NH ALLO)				
Middle frontal gyrus (MFG)	R	45, 9, 42	4.71	162
Inferior parietal lobe (IPL)	R	45, −54, 51	4.07	114
Superior frontal gyrus (SFG)	R	24, 15, 63	3.58	68
STG→FPN				
(DHH EGO > NH EGO) exclusively masked by (DHH ALLO > NH ALLO)				
Superior temporal gyrus (STG)	R	60, −24, 9	4.00	60
	L	−60, −27, 9	3.66	44
(C) PC between STG and DMN				
DMN→STG				
(DHH EGO > NH EGO) exclusively masked by (DHH ALLO > NH ALLO)				
Cuneus	R	12, −57, 21	3.86	78
Precuneus	*M*	*3, −60, 30*	3.28	
Medial prefrontal cortex (mPFC)	M	9, 45, −12	3.21	51
STG→DMN				
(DHH EGO > NH EGO) exclusively masked by (DHH ALLO > NH ALLO)				
Superior temporal gyrus (STG)	R	60, −27, 6	3.19	39

Italics indicate the coordinates of relevant local maxima within each significant cluster. DAN, dorsal attention network; FPN, frontoparietal network; DMN, default-mode network; ALLO, allocentric task; EGO, egocentric task; DHH, deaf and early hard of hearing; NH, normal hearing; L, left; R, right.

Discussion

Body-centered visuomotor transformation during egocentric judgments is impaired after early auditory deprivation (Li et al. 2022). This behavioral impairment is associated with increased inter-network connectivity beyond the auditory system, particularly between the DMN and the task-relevant networks in the DAN and FPN (Li et al. 2022). It remains unknown, however, whether and how the large-scale reorganization involving the auditory cortex is associated with impaired egocentric spatial processing after early auditory deprivation. Here, we investigated the cross-modal reorganization in the auditory cortex of DHH people during body-centered visuomotor transformation focusing on altered neural network dynamics between the auditory cortex in the bilateral STG, the task-critical networks in the DAN and FPN, and the DMN during the egocentric task, compared with the allocentric task.

Morphologically, we observed increased cortical thickness in the left STG of the DHH group (Fig. 2A). Previous surface-based morphometry studies with a relatively small sample size (<16 participants per group) showed no significant difference in the cortical thickness of the auditory regions between the DHH and NH groups (Li et al. 2012; Hribar et al. 2014; Smittenaar et al. 2016). A recent meta-analysis did not provide any clear outcome (Manno et al. 2021). This lack of significant differences is likely because the cortical folds in the temporal lobe are inconsistent across individuals. Thus larger sample sizes may be required to detect temporal lobe thickness changes (Pardoe et al. 2012). Accordingly, two recent studies with larger sample sizes (30 and 50 participants per group, respectively) showed that the cortical thickness of the STG increased in DHH relative to NH people (Kumar and Mishra 2018; McCullough and Emmorey 2020). Loss of sensory input produces comparatively mild effects on synapse development (Winfield 1981, 1983; Bourgeois et al. 1989; Bourgeois and Rakic 1996; Kral et al. 2005). Instead, the subsequent synaptic pruning with removing unnecessary synapses and neurons, which may be related to cortical thinning, is supported by sensory experiences (Bourgeois et al. 1989; Bourgeois and Rakic 1996; Yu et al. 2013; Faust et al. 2021). Accordingly, early auditory deprivation leads to inadequate synaptic pruning. Also, myelination is associated with cortical thickness (Sowell et al. 2004; Natu et al. 2019), and previous evidence has shown a decreased myelination both in auditory (Emmorey et al. 2003; Hribar et al. 2014; Karns et al. 2016) and visual deprivation (Winfield 1983). Furthermore, abnormal cortical thickness may be related to cortical malformation (Hyde et al. 2007; Hogstrom et al. 2012). In the tension-based theory, cortical folding can be explained by mechanical tension along axons, dendrites, and glial processes (Van Essen 1997). Early auditory deprivation may change the tonotopic organization of a DHH individual's brain, related to a thicker auditory cortex (for review, Hribar et al. 2020). Therefore, the increased cortical thickness of the auditory cortex in the DHH participants' brains might imply that the lack of early auditory input results in inadequate synaptic pruning, demyelination, and cortical malformation. The cortical thickness of the left STG in the DHH participants exhibited a trend of positive correlation with their egocentric performance (Supplementary Fig. 1), indicating that as the cortical thickness of the auditory cortex increases in the DHH participants, the impairments in egocentric processing may become more severe. Functionally, we found that the auditory cortex in bilateral STG of the DHH was generally hyper-activated during all three visual tasks, as compared with the NH controls (Fig. 2B). Early auditory deprivation alters an individual's interaction with the external

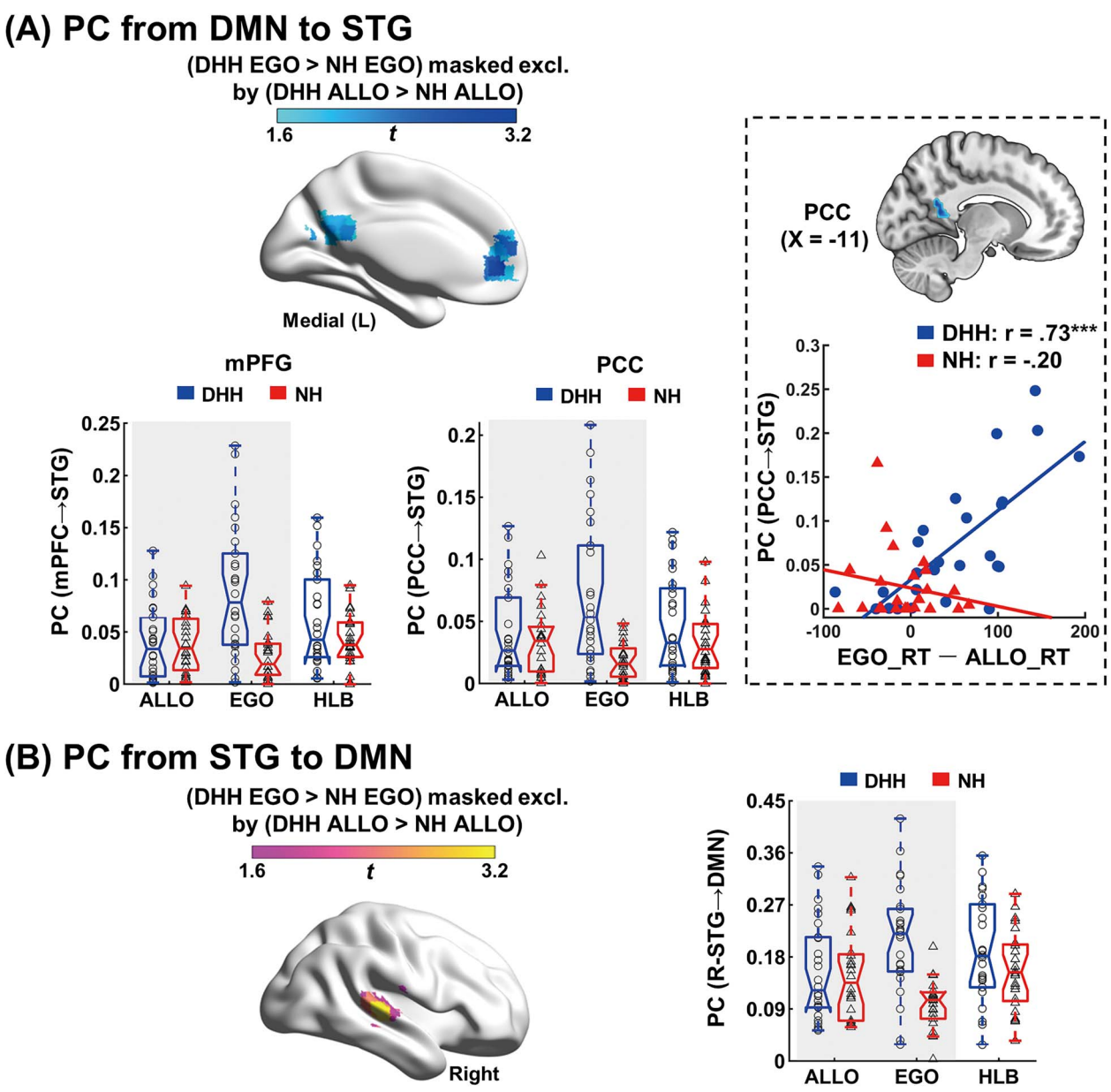

Fig. 7. Task-state PC results between the STG and the DMN. A) PC from the DMN to the STG. Left panel: the interaction effect between the subject group (DHH vs. NH) and the visual tasks (EGO vs. ALLO). Both the mPFC and the PCC in the DMN showed significantly stronger PC values with the STG in the DHH than the NH group, especially during the egocentric rather than the allocentric task. Moreover, the PC value from the PCC in the DMN to the STG was significantly positively correlated with the egocentric performance ("EGO_RT – ALLO_RT") only in the DHH group but not in the NH group (right panel). The stronger the PCC-STG connectivity in a DHH individual, the slower the egocentric judgment. ***$P < 0.001$. B) PC from the STG to the DMN. The right STG showed significantly stronger PC values with the DMN in the DHH than the NH group during the egocentric rather than allocentric task. For demonstration purposes, mean PC values were extracted from the significantly activated regions and shown as a function of the three tasks in each subject group. No further statistical analysis was performed on the extracted PC values to avoid double-dipping. The conditions involved in the neural contrast were shaded. ALLO, allocentric task; EGO, egocentric task; L, left.

environment, which leads to a striking functional reorganization in the auditory system. Accordingly, mounting empirical evidence shows that the "deprived" auditory cortex of DHH people is recruited by the remaining senses, such as visual and vibrotactile stimuli (Bavelier et al. 2000, 2001; Fine et al. 2005; Karns et al. 2012; Cardin et al. 2013, 2018; Ding et al. 2015; Benetti et al. 2017, 2021).

Besides hearing loss, we cannot rule out the effects of sign-language experiences since all DHH participants in the present study were sign-language users. Sign language, a visuospatial language that exploits visual imagery, space, and movement (MacSweeney et al. 2008), has been shown to enhance an individual's visuospatial representations (Emmorey 2002; Keehner and Gathercole 2007; Pyers et al. 2010). During a mental rotation task, researchers found that DHH and NH signers were faster for object rotation than NH nonsigners (Emmorey et al. 1993). Previous studies suggest that objects are encoded in allocentric and egocentric reference frames, with the former predominating during mental rotation (Corballis et al. 1976, 1978). Therefore, signers' enhanced mental rotation abilities may be related to a more critical reliance on the allocentric reference frame (Masataka 1995). Interestingly, a recent study found that as the proficiency of learned sign language increases,

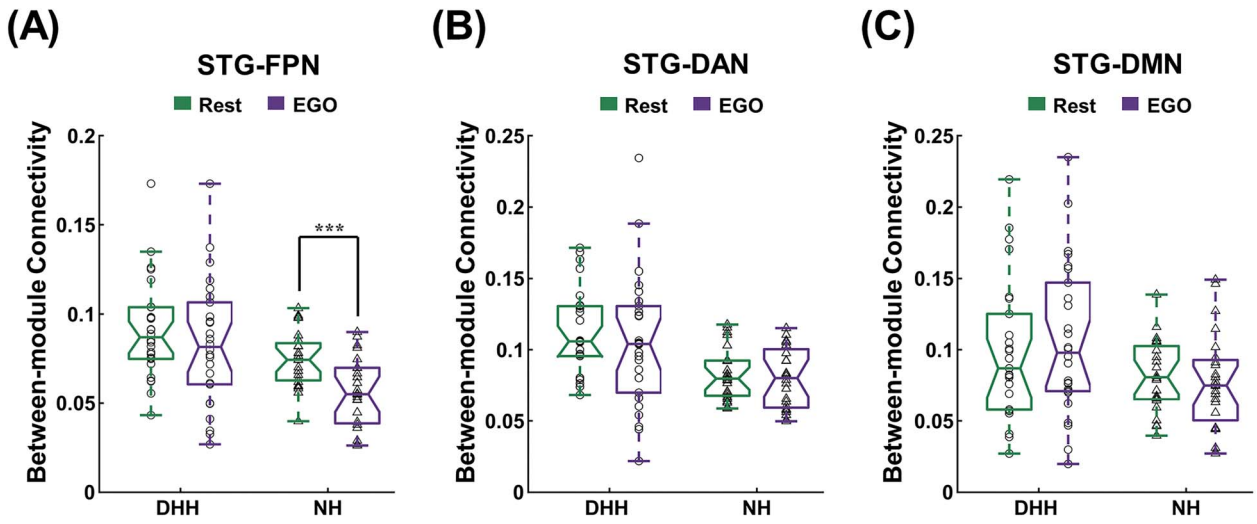

Fig. 8. Alterations in between-module connectivity during the egocentric task relative to the resting state in the two subject groups. A) STG-FPN. B) STG-DAN. c) STG-DMN. ***$P < 0.001$. EGO, egocentric task.

the superior lateral occipital cortex (LOC) exhibited a more robust connectivity with the high-level language region (i.e. IFG) during a sign-related semantic judgment task (Banaszkiewicz et al. 2021). The superior LOC codes visuospatial representations during allocentric judgments (Committeri et al. 2004; Zaehle et al. 2007; Chen et al. 2012). Therefore, the findings mentioned before imply that sign-language experiences might promote the dominance of the allocentric reference frame. Accordingly, we speculate that the egocentric reference frame might be compromised by the dominating allocentric reference frame in DHH people using sign language. Moreover, as sign language fluency increases, the allocentric reference frame might become more dominant, further impairing the function of the egocentric reference frame. To compensate for the impaired egocentric processing potentially caused by sign language use, the STG might become more integrated with the task-critical FPN during the egocentric task (Fig. 6). The effect of sign language on the cortical reorganization involving the STG remains controversial. Some researchers have found that sign language plays an essential role in the neural plasticity of the STG in the DHH (Neville et al. 1998; Petitto et al. 2000; Sadato et al. 2004; Cardin et al. 2013), an effect that could not be observed in other studies (Bavelier et al. 2001; MacSweeney et al. 2004; Fine et al. 2005; Olulade et al. 2014; Twomey et al. 2017). Therefore, sign language might explain some of the present results. Further research with DHH signers, NH signers, and NH nonsigners is warranted to tease apart the effect of early auditory deprivation vs. sign-language experience on the large-scale functional reorganization of the auditory system during the egocentric task. Please also note that vestibular deficits have a high comorbidity rate with hearing loss (Moïn-Darbari et al. 2021). Moreover, the STG has been proven to be part of the vestibular cortical network (Bense et al. 2004; Dieterich and Brandt 2008, 2015; Helmchen et al. 2009; Lopez et al. 2012), and vestibular compensation has been associated with network reorganization involving the auditory system (Grosch et al. 2021). Although the DHH participants in the present study reported no subjectively experienced balance problems, they might have undetected vestibular impairment (Tamaki et al. 2021). Therefore, putative deficits of vestibular functions might explain some of the present results involving the STG. Further work will need to tease apart the effect of early auditory deprivation vs. vestibular deficits on the large-scale network reorganization underlying the impaired egocentric processing in the DHH people.

The functional cross-modal reorganization in the DHH is not only confined within the auditory system but also manifests as altered cortico-cortical connectivity between the auditory cortex and other cortical regions during a variety of visual tasks (Bavelier et al. 2000; Shiell et al. 2015; Benetti et al. 2017, 2021; Bola et al. 2017). It remains unclear, however, whether the altered neural network dynamics between the STG and other cortical areas were beneficial or detrimental to a specific visual task. In the present study, the auditory system in the bilateral STG showed enhanced functional connectivity with the DAN and the FPN in the DHH people (compared with the NH controls) during the resting state (Fig. 4) and the egocentric task (Figs. 5 and 6). Moreover, the stronger the functional connectivity during the egocentric task between the STG and the DAN and between the STG and the FPN, the better DHH persons performed in the egocentric task (Figs 5A and 6A, the right panel). This finding indicates a beneficial role of enhanced STG-task network connectivity. Previous studies suggest that during the egocentric task, the DAN supports general visuospatial representations (Committeri et al. 2004; Chen et al. 2012, 2014; Gomez et al. 2014; Liu, Li, et al. 2017), whereas the FPN supports the body-centered visuomotor transformation (Galati et al. 2000; Neggers et al. 2006; Chen et al. 2012, 2014; Liu, Li, et al. 2017). In order to ensure efficient task performance, the task-relevant regions are highly connected to maintain the high modularity of the task-relevant network; meanwhile, the task-relevant regions are disconnected from the task-irrelevant regions (Ekman et al. 2012; Gratton et al. 2016). In the present study, the STG was not involved in the egocentric task for the NH controls (Fig. 2B), i.e. a task-irrelevant area. Because of environmental noise, e.g. the scanner noise in the present fMRI study, the auditory system in the STG may even act as a distracting region during the egocentric task for the NH controls. Thus, to ensure efficient egocentric judgments, the task-critical FPN needs to be highly segregated/disconnected from the auditory system (Figs. 6 and 8A). For DHH individuals, however, both the reorganized auditory system in the STG and the task-relevant DAN and FPN were involved in the egocentric task (Figs. 2B and 3A). Therefore, the neural coupling between the STG, the DAN and the FPN was enhanced to optimize the egocentric performance: the higher the neural

coupling, the better the egocentric performance in the DHH people (Figs. 5A and 6A, the right panel). Previous evidence suggests a beneficial role of increased functional connectivity between task-related networks during near-threshold perception (Weisz et al. 2014; Leske et al. 2015; Sadaghiani et al. 2015), visual attention (Spadone et al. 2015), and working memory (Braun et al. 2015; Shine et al. 2016). However, it remains unclear how such increased interaction between task-related networks impacts spatial reference frame tasks. In the present study, the STG of the DHH people showed increased connectivity with the task-related DAN and FPN during the egocentric task. The increased integration between task-related regions is crucial for recruiting necessary resources and optimizing widespread communications (Shine et al. 2016; Gonzalez-Castillo and Bandettini 2018; Menon and D'Esposito 2022). Accordingly, the efficient information flow between the STG and the cortical areas underlying the egocentric reference frame might facilitate body-centered visuomotor transformations, mitigating the impaired egocentric processing after early auditory deprivation.

On the other hand, the auditory cortex of the DHH group also showed enhanced connectivity with the task-irrelevant DMN during the egocentric task (Fig. 7). In contrast to the enhanced STG-task-relevant network connectivity, the enhanced STG-task-irrelevant DMN connectivity was associated with an impaired egocentric performance of the DHH people: the stronger the STG-DMN connectivity, the worse the egocentric performance in the DHH people (Fig. 7A, the right panel). The DMN is generally deactivated during various externally directed tasks to suppress task-irrelevant distractions (Shulman et al. 1997; Gusnard and Raichle 2001; Raichle et al. 2001; Fox et al. 2005). Therefore, a stronger anticorrelation between the DMN and the task-positive networks predicts better task performance (Sala-Llonch et al. 2012; Thompson et al. 2013). Furthermore, previous evidence shows that efficient task performance is associated with stronger modularity in the task-negative DMN in terms of lower between-module connectivity between the DMN and the task-relevant neural networks and higher within-module connectivity in the DMN (Weisz et al. 2014; Sadaghiani et al. 2015; Gonzalez-Castillo and Bandettini 2018). It has been suggested that the DAN and the FPN, two task-critical networks supporting the egocentric task, show stronger functional and structural connectivity with the DMN in DHH people (Dell Ducas et al. 2021; Li et al. 2022). Moreover, increased inter-network connectivity between the task-irrelevant DMN and the task-relevant DAN and FPN was associated with impaired egocentric performance in DHH people (Li et al. 2022). Given that the DHH participants' STG became more integrated with the task-relevant DAN and FPN to improve the egocentric processing (Figs. 5 and 6), the increased neural coupling between the task-relevant STG and the task-irrelevant DMN interfered with the egocentric processing, resulting in detrimental egocentric performance in the DHH people (Fig. 7).

To summarize, we revealed extensively reorganized inter-module connectivity between the auditory system in the bilateral STG, the task-relevant DAN and FPN, and the task-irrelevant DMN in the DHH people during body-centered visuomotor transformation. The STG in the DHH people becomes more integrated with the task-relevant regions in the DAN and FPN during the egocentric task. Accordingly, the more robust connectivity between the STG of DHH people and the task-relevant networks was associated with enhanced egocentric performance. In comparison, the stronger connectivity between the STG of DHH people and the task-negative DMN was associated with deteriorated egocentric performance.

Acknowledgments

The authors also wish to thank all of participants who volunteered their time without whom this project would not have been possible.

Author contributions

Li Song (Formal analysis, Methodology, Visualization, Writing—original draft, Writing—review & editing), Pengfei Wang (Data curation, Methodology, Supervision, Validation), Hui Li (Data curation, Investigation, Software, Supervision, Validation), Peter Weiss (Supervision, Validation, Writing—review & editing), Gereon R. Fink (Conceptualization, Supervision, Validation, Writing—review & editing), Xiaolin Zhou (Conceptualization, Supervision, Validation, Writing—review & editing), and Qi Chen (Conceptualization, Funding acquisition, Project administration, Resources, Supervision, Validation, Writing—review & editing)

Supplementary material

Supplementary material is available at *Cerebral Cortex* online.

Funding

The Natural Science Foundation of China (31871138, 32071052); the MOE Project of Key Research Institute of Humanities and Social Sciences in Universities (22JJD190006).

Conflict of interest statement: None declared.

Data and code availability

All the data and code are available at https://osf.io/du3rt/. The data and code used in the study are available in the public domain for its sharing or re-use. The data and code sharing adopted by the authors comply with the requirements of the institute and comply with institutional ethics approval.

References

Alavash M, Tune S, Obleser J. Modular reconfiguration of an auditory control brasin network supports adaptive listening behavior. *Proc Natl Acad Sci U S A*. 2019:116:660–669.

Amaral L, Almeida J. Neuroplasticity in congenitally deaf humans. *Rev Port Psicol*. 2015:44:121–132.

Anderson JS, Druzgal TJ, Lopez-Larson M, Jeong EK, Desai K, Yurgelun-Todd D. Network anticorrelations, global regression, and phase-shifted soft tissue correction. *Hum Brain Mapp*. 2011:32:919–934.

Andin J, Holmer E. Reorganization of large-scale brain networks in deaf signing adults: the role of auditory cortex in functional reorganization following deafness. *Neuropsychologia*. 2022:166:108139.

Banaszkiewicz A, Matuszewski J, Bola Ł, Szczepanik M, Kossowski B, Rutkowski P, Szwed M, Emmorey K, Jednoróg K, Marchewka A. Multimodal imaging of brain reorganization in hearing late learners of sign language. *Hum Brain Mapp*. 2021:42:384–397.

Baum GL, Ciric R, Roalf DR, Betzel RF, Moore TM, Shinohara RT, Kahn AE, Vandekar SN, Rupert PE, Quarmley M, et al. Modular segregation of structural brain networks supports the development of executive function in youth. *Curr Biol*. 2017:27:1561–1572.e8.

Bavelier D, Tomann A, Hutton C, Mitchell T, Corina D, Liu G, Neville H. Visual attention to the periphery is enhanced in congenitally deaf individuals. *J Neurosci*. 2000:20:1–6.

Bavelier D, Brozinsky C, Tomann A, Mitchell T, Neville H, Liu G. Impact of early deafness and early exposure to sign language on the cerebral organization for motion processing. *J Neurosci*. 2001:21:8931–8942.

Benetti S, Van Ackeren MJ, Rabini G, Zonca J, Foa V, Baruffaldi F, Rezk M, Pavani F, Rossion B, Collignon O. Functional selectivity for face processing in the temporal voice area of early deaf individuals. *Proc Natl Acad Sci U S A*. 2017:114:E6437–E6446.

Benetti S, Zonca J, Ferrari A, Rezk M, Rabini G, Collignon O. Visual motion processing recruits regions selective for auditory motion in early deaf individuals. *NeuroImage*. 2021:230:117816.

Bense S, Bartenstein P, Lochmann M, Schlindwein P, Brandt T, Dieterich M. Metabolic changes in vestibular and visual cortices in acute vestibular neuritis. *Ann Neurol*. 2004:56:624–630.

Betzel RF, Griffa A, Hagmann P, Misic B. Distance-dependent consensus thresholds for generating group-representative structural brain networks. *Netw Neurosci*. 2019:3:475–496.

Blouin J, Bard C, Teasdale N, Paillard J, Fleury M, Forget R, Lamarre Y. Reference systems for coding spatial information in normal subjects and a deafferented patient. *Exp Brain Res*. 1993:93:324–331.

Bola Ł, Zimmermann M, Mostowski P, Jednoróg K, Marchewka A, Rutkowski P, Szwed M. Task-specific reorganization of the auditory cortex in deaf humans. *Proc Natl Acad Sci U S A*. 2017:114:E600–E609.

Bourgeois JP, Rakic P. Synaptogenesis in the occipital cortex of macaque monkey devoid of retinal input from early embryonic stages. *Eur J Neurosci*. 1996:8:942–950.

Bourgeois JP, Jastreboff PJ, Rakic P. Synaptogenesis in visual cortex of normal and preterm monkeys: evidence for intrinsic regulation of synaptic overproduction. *Proc Natl Acad Sci U S A*. 1989:86:4297–4301.

Braun U, Schäfer A, Walter H, Erk S, Romanczuk-Seiferth N, Haddad L, Schweiger JI, Grimm O, Heinz A, Tost H, et al. Dynamic reconfiguration of frontal brain networks during executive cognition in humans. *Proc Natl Acad Sci U S A*. 2015:112:11678–11683.

Burgess N. Spatial memory: how egocentric and allocentric combine. *Trends Cogn Sci*. 2006:10:551–557.

Cardin V, Orfanidou E, Rönnberg J, Capek CM, Rudner M, Woll B. Dissociating cognitive and sensory neural plasticity in human superior temporal cortex. *Nat Commun*. 2013:4(1):1473.

Cardin V, Rudner M, De Oliveira RF, Andin J, Su MT, Beese L, Woll B, Rönnberg J. The organization of working memory networks is shaped by early sensory experience. *Cereb Cortex*. 2018:28:3540–3554.

Cardin V, Grin K, Vinogradova V, Manini B. Crossmodal reorganisation in deafness: mechanisms for functional preservation and functional change. *Neurosci Biobehav Rev*. 2020:113:227–237.

Chen Q, Weidner R, Weiss PH, Marshall JC, Fink GR. Neural interaction between spatial domain and spatial reference frame in parietal–occipital junction. *J Cogn Neurosci*. 2012:24:2223–2236.

Chen Y, Monaco S, Byrne P, Yan X, Henriques DYP, Douglas CJ. Allocentric versus egocentric representation of remembered reach targets in human cortex. *J Neurosci*. 2014:34:12515–12526.

Cohen YE, Andersen RA. A common reference frame for movement plans in the posterior parietal cortex. *Nat Rev Neurosci*. 2002:3:553–562.

Cole MW, Bassett DS, Power JD, Braver TS, Petersen SE. Intrinsic and task-evoked network architectures of the human brain. *Neuron*. 2014:83:238–251.

Cole MW, Ito T, Bassett DS, Schultz DH. Activity flow over resting-state networks shapes cognitive task activations. *Nat Neurosci*. 2016:19:1718–1726.

Committeri G, Galati G, Paradis AL, Pizzamiglio L, Berthoz A, LeBihan D. Reference frames for spatial cognition: different brain areas are involved in viewer-, object-, and landmark-centered judgments about object location. *J Cogn Neurosci*. 2004:16:1517–1535.

Corballis MC, Zbrodoff J, Roldan CE. What's up in mental rotation? *Percept Psychophys*. 1976:19:525–530.

Corballis MC, Nagourney BA, Shetzer LI, Stefanatos G. Mental rotation under head tilt: factors influencing the location of the subjective reference frame. *Percept Psychophys*. 1978:24:263–273.

Dahnke R, Yotter RA, Gaser C. Cortical thickness and central surface estimation. *NeuroImage*. 2013:65:336–348.

Damoiseaux JS, Rombouts SARB, Barkhof F, Scheltens P, Stam CJ, Smith SM, Beckmann CF. Consistent resting-state networks across healthy subjects. *Proc Natl Acad Sci*. 2006:103:13848–13853.

De Luca M, Beckmann CF, De Stefano N, Matthews PM, Smith SM. fMRI resting state networks define distinct modes of long-distance interactions in the human brain. *NeuroImage*. 2006:29:1359–1367.

Dell Ducas K, Senra Filho A da, Silva PR, Secchinato KF, Leoni RF, Santos ACS. 2021. Functional and structural brain connectivity in congenital deafness. *Brain Struct Funct* 226:1323–1333.

Dieterich M, Brandt T. Functional brain imaging of peripheral and central vestibular disorders. *Brain*. 2008:131:2538–2552.

Dieterich M, Brandt T. The bilateral central vestibular system: its pathways, functions, and disorders. *Ann N Y Acad Sci*. 2015:1343:10–26.

Ding H, Qin W, Liang M, Ming D, Wan B, Li Q, Yu C. Cross-modal activation of auditory regions during visuo-spatial working memory in early deafness. *Brain*. 2015:138:2750–2765.

Ding H, Ming D, Wan B, Li Q, Qin W, Yu C. Enhanced spontaneous functional connectivity of the superior temporal gyrus in early deafness. *Sci Rep*. 2016:6:1–11.

Ekman M, Derrfuss J, Tittgemeyer M, Fiebach CJ. Predicting errors from reconfiguration patterns in human brain networks. *Proc Natl Acad Sci U S A*. 2012:109:16714–16719.

Emmorey K. *Language, cognition, and the brain: insights from sign language research*. Mahwah, NJ: Lawrence Erlbaum Associates; 2002.

Emmorey K, Kosslyn SM, Bellugi U. Visual imagery and visual-spatial language: enhanced imagery abilities in deaf and hearing ASL signers. *Cognition*. 1993:46:139–181.

Emmorey K, Allen JS, Bruss J, Schenker N, Emmorey K, Allen JS, Bruss J, Schenker N, Damasio H. A morphometric analysis of auditory brain regions in congenitally deaf adults. *Proc Natl Acad Sci U S A*. 2003:100:10049–10054.

Faust T, Gunner G, Schafer DP. Mechanisms governing activity-dependent synaptic pruning in the developing mammalian CNS. *Nat Rev Neurosci*. 2021:22:657–673.

Findlay JM. Saccade target selection during visual search. *Vis Res*. 1997:37:617–631.

Fine I, Finney EM, Boynton GM, Dobkins KR. Comparing the effects of auditory deprivation and sign language within the auditory and visual cortex. *J Cogn Neurosci*. 2005:17:1621–1637.

Fornito A, Zalesky A, Pantelis C, Bullmore ET. Schizophrenia, neuroimaging and connectomics. *NeuroImage*. 2012:62:2296–2314.

Fortunato S. Community detection in graphs. *Phys Rep*. 2010:486:75–174.

Fox MD, Raichle ME. Spontaneous fluctuations in brain activity observed with functional magnetic resonance imaging. *Nat Rev Neurosci*. 2007:8:700–711.

Fox MD, Snyder AZ, Vincent JL, Corbetta M, Van Essen DC, Raichle ME. The human brain is intrinsically organized into dynamic, anticorrelated functional networks. *Proc Natl Acad Sci U S A*. 2005:102:9673–9678.

Galati G, Lobel E, Vallar G, Berthoz A, Pizzamiglio L, Le BD. The neural basis of egocentric and allocentric coding of space in humans: a functional magnetic resonance study. *Exp Brain Res*. 2000:133: 156–164.

Galati G, Committeri G, Sanes JN, Pizzamiglio L. Spatial coding of visual and somatic sensory information in body-centred coordinates. *Eur J Neurosci*. 2001:14:737–746.

Gandemer L, Parseihian G, Kronland-Martinet R, Bourdin C. Spatial cues provided by sound improve postural stabilization: evidence of a spatial auditory map? *Front Neurosci*. 2017:11:1–11.

Geerligs L, Renken RJ, Saliasi E, Maurits NM, Lorist MM. A brain-wide study of age-related changes in functional connectivity. *Cereb Cortex*. 2015:25:1987–1999.

Gomez A, Cerles M, Rousset S, Rémy C, Baciu M. Differential hippocampal and retrosplenial involvement in egocentric-updating, rotation, and allocentric processing during online spatial encoding: an fMRI study. *Front Hum Neurosci*. 2014:8:1–14.

Gonzalez-Castillo J, Bandettini PA. Task-based dynamic functional connectivity: recent findings and open questions. *NeuroImage*. 2018:180:526–533.

Gordon EM, Laumann TO, Gilmore AW, Newbold DJ, Greene DJ, Berg JJ, Ortega M, Hoyt-Drazen C, Gratton C, Sun H, et al. Precision functional mapping of individual human brains. *Neuron*. 2017:95: 791–807.

Gratton C, Nomura EM, Pérez F, D'Esposito M. Focal brain lesions to critical locations cause widespread disruption of the modular organization of the brain. *J Cogn Neurosci*. 2012:24:1275–1285.

Gratton C, Laumann TO, Gordon EM, Adeyemo B, Petersen SE. Evidence for two independent factors that modify brain networks to meet task goals. *Cell Rep*. 2016:17:1276–1288.

Grosch M, Lindner M, Bartenstein P, Brandt T, Dieterich M, Ziegler S, Zwergal A. Dynamic whole-brain metabolic connectivity during vestibular compensation in the rat. *NeuroImage*. 2021:226: 117588.

Guimerà R, Amaral LAN. Functional cartography of complex metabolic networks. *Nature*. 2005:433:895–900.

Guo X, Simas T, Lai MC, Lombardo MV, Chakrabarti B, Ruigrok ANV, Bullmore ET, Baron-Cohen S, Chen H, Suckling J. Enhancement of indirect functional connections with shortest path length in the adult autistic brain. *Hum Brain Mapp*. 2019:40:5354–5369.

Gusnard DA, Raichle ME. Searching for a baseline: functional imaging and the human brain. *Neuroscience*. 2001:2:685–694.

Hearne LJ, Cocchi L, Zalesky A, Mattingley JB. Reconfiguration of brain network architectures between resting-state and complexity-dependent cognitive reasoning. *J Neurosci*. 2017:37: 8399–8411.

Helmchen C, Klinkenstein J, MacHner B, Rambold H, Mohr C, Sander T. Structural changes in the human brain following vestibular neuritis indicate central vestibular compensation. *Ann N Y Acad Sci*. 2009:1164:104–115.

Helwegen K, Libedinsky I, van den Heuvel MP. Statistical power in network neuroscience. *Trends Cogn Sci*. 2023:27:282–301.

van den Heuvel MP, de Lange SC, Zalesky A, Seguin C, Yeo BTT, Schmidt R. Proportional thresholding in resting-state fMRI functional connectivity networks and consequences for patient-control connectome studies: issues and recommendations. *NeuroImage*. 2017:152:437–449.

Hogstrom LJ, Westlye LT, Walhovd KB, Fjell AM. The structure of the cerebral cortex across adult life: age-related patterns of surface area, thickness, and gyrification. *Cereb Cortex*. 2012:23: 2521–2530.

Houde MS, Landry SP, Page S, Maheu M, Champoux F. Body perception and action following deafness. *Neural Plast*. 2016:2016:1–7.

Hribar M, Šuput D, Carvalho AA, Battelino S, Vovk A. Structural alterations of brain grey and white matter in early deaf adults. *Hear Res*. 2014:318:1–10.

Hribar M, Šuput D, Battelino S, Vovk A. Review article: structural brain alterations in prelingually deaf. *NeuroImage*. 2020:220:117042.

Hyde KL, Lerch JP, Zatorre RJ, Griffiths TD, Evans AC, Peretz I. Cortical thickness in congenital amusia: when less is better than more. *J Neurosci*. 2007:27:13028–13032.

Kanegaonkar RG, Amin K, Clarke M. The contribution of hearing to normal balance. *J Laryngol Otol*. 2012:126:984–988.

Karns CM, Dow MW, Neville HJ. Altered cross-modal processing in the primary auditory cortex of congenitally deaf adults: a visual-somatosensory fMRI study with a double-flash illusion. *J Neurosci*. 2012:32:9626–9638.

Karns CM, Stevens C, Dow MW, Schorr EM, Neville HJ. Atypical white-matter microstructure in congenitally deaf adults: a region of interest and tractography study using diffusion-tensor imaging. *Hear Res*. 2016:343:72–82.

Keehner M, Gathercole SE. Cognitive adaptations arising from non-native experience of sign language in hearing adults. *Mem Cogn*. 2007:35:752–761.

Keller CJ, Bickel S, Honey CJ, Groppe DM, Entz L, Craddock RC, Lado FA, Kelly C, Milham M, Mehta AD. Neurophysiological investigation of spontaneous correlated and anticorrelated fluctuations of the BOLD signal. *J Neurosci*. 2013:33:6333–6342.

Kral A, Tillein J, Heid S, Hartmann R, Klinke R. Postnatal cortical development in congenital auditory deprivation. *Cereb Cortex*. 2005:15:552–562.

Kral A, Kronenberger WG, Pisoni DB, O'Donoghue GM. Neurocognitive factors in sensory restoration of early deafness: a connectome model. *Lancet Neurol*. 2016:15:610–621.

Kriegeskorte N, Simmons WK, Bellgowan PS, Baker CI. Circular analysis in systems neuroscience: the dangers of double dipping. *Nat Neurosci*. 2009:12:535–540.

Kriegeskorte N, Lindquist MA, Nichols TE, Poldrack RA, Vul E. Everything you never wanted to know about circular analysis, but were afraid to ask. *J Cereb Blood Flow Metab*. 2010:30:1551–1557.

Kronenberger WG, Beer J, Castellanos I, Pisoni DB, Miyamoto RT. Neurocognitive risk in children with cochlear implants. *JAMA Otolaryngol Head Neck Surg*. 2014:140:608–615.

Kumar U, Mishra M. Pattern of neural divergence in adults with prelingual deafness: based on structural brain analysis. *Brain Res*. 2018:1701:58–63.

Lei T, Liao X, Chen X, Zhao T, Xu Y, Xia M, Zhang J, Xia Y, Sun X, Wei Y, et al. Progressive stabilization of brain network dynamics during childhood and adolescence. *Cereb Cortex*. 2022:32: 1024–1039.

Leske S, Ruhnau P, Frey J, Lithari C, Müller N, Hartmann T, Weisz N. Prestimulus network integration of auditory cortex predisposes near-threshold perception independently of local excitability. *Cereb Cortex*. 2015:25:4898–4907.

Levänen S, Jousmäki V, Hari R. Vibration-induced auditory-cortex activation in a congenitally deaf adult. *Curr Biol*. 1998:8:869–872.

Li J, Li W, Xian J, Li Y, Liu Z, Liu S, Wang X, Wang Z, He H. Cortical thickness analysis and optimized voxel-based morphometry in children and adolescents with prelingually profound sensorineural hearing loss. *Brain Res*. 2012:1430:35–42.

Li H, Song L, Wang P, Weiss PH, Fink GR, Zhou X, Chen Q. Impaired body-centered sensorimotor transformations in congenitally deaf people. *Brain Commun*. 2022:4:fcac148.

Liang X, Zou Q, He Y, Yang Y. Topologically reorganized connectivity architecture of default-mode, executive-control, and

salience networks across working memory task loads. *Cereb Cortex*. 2016:26:1501–1511.
Liu N, Li H, Su W, Chen Q. Common and specific neural correlates underlying the spatial congruency effect induced by the egocentric and allocentric reference frame. *Hum Brain Mapp*. 2017:38: 2112–2127.
Liu TT, Nalci A, Falahpour M. The global signal in fMRI: nuisance or information? *NeuroImage*. 2017:150:213–229.
Liu J, Xia M, Wang X, Liao X, He Y. The spatial organization of the chronnectome associates with cortical hierarchy and transcriptional profiles in the human brain. *NeuroImage*. 2020:222:117296.
Lopez C, Blanke O, Mast FW. The human vestibular cortex revealed by coordinate-based activation likelihood estimation meta-analysis. *Neuroscience*. 2012:212:159–179.
Ma Q, Tang Y, Wang F, Liao X, Jiang X, Wei S, Mechelli A, He Y, Xia M. Transdiagnostic dysfunctions in brain modules across patients with schizophrenia, bipolar disorder, and major depressive disorder: a connectome-based study. *Schizophr Bull*. 2020:46:699–712.
MacSweeney M, Campbell R, Woll B, Giampietro V, David AS, McGuire PK, Calvert GA, Brammer MJ. Dissociating linguistic and nonlinguistic gestural communication in the brain. *NeuroImage*. 2004:22: 1605–1618.
MacSweeney M, Capek CM, Campbell R, Woll B. The signing brain: the neurobiology of sign language. *Trends Cogn Sci*. 2008:12:432–440.
Manno FAM, Rodríguez-Cruces R, Kumar R, Ratnanather JT, Lau C. Hearing loss impacts gray and white matter across the lifespan: systematic review, meta-analysis and meta-regression. *NeuroImage*. 2021:231:117826.
Masataka N. Absence of mirror-reversal tendency in cutaneous pattern perception and acquisition of a signed language in deaf children. *Br J Dev Psychol*. 1995:13:97–106.
McCullough S, Emmorey K. Effects of deafness and sign language experience on the human brain: voxel-based and surface-based morphometry. *Lang Cogn Neurosci*. 2020:36:422–439.
Menon V, D'Esposito M. The role of PFC networks in cognitive control and executive function. *Neuropsychopharmacology*. 2022:47:90–103.
Meunier D, Achard S, Morcom A, Bullmore E. Age-related changes in modular organization of human brain functional networks. *NeuroImage*. 2009:44:715–723.
Moïn-Darbari K, Lafontaine L, Maheu M, Bacon BA, Champoux F. Vestibular status: a missing factor in our understanding of brain reorganization in deaf individuals. *Cortex*. 2021:138:311–317.
Morosan P, Rademacher J, Schleicher A, Amunts K, Schormann T, Zilles K. Human primary auditory cortex: cytoarchitectonic subdivisions and mapping into a spatial reference system. *NeuroImage*. 2001:13:684–701.
Morosan P, Schleicher A, Amunts K, Zilles K. Multimodal architectonic mapping of human superior temporal gyrus. *Anat Embryol (Berl)*. 2005:210:401–406.
Mostofsky SH, Powell SK, Simmonds DJ, Goldberg MC, Caffo B, Pekar JJ. Decreased connectivity and cerebellar activity in autism during motor task performance. *Brain*. 2009:132:2413–2425.
Murphy K, Fox MD. Towards a consensus regarding global signal regression for resting state functional connectivity MRI. *NeuroImage*. 2017:154:169–173.
Murphy K, Birn RM, Handwerker DA, Jones TB, Bandettini PA. The impact of global signal regression on resting state correlations: are anti-correlated networks introduced? *NeuroImage*. 2009:44: 893–905.
Natu VS, Gomez J, Barnett M, Jeska B, Kirilina E, Jaeger C, Zhen Z, Cox S, Weiner KS, Weiskopf N, et al. Apparent thinning of human visual cortex during childhood is associated with myelination. *Proc Natl Acad Sci U S A*. 2019:116:20750–20759.
Neggers SFW, Van der Lubbe RHJ, Ramsey NF, Postma A. Interactions between ego- and allocentric neuronal representations of space. *NeuroImage*. 2006:31:320–331.
Neville HJ, Bavelier D, Corina D, Rauschecker J, Karni A, Lalwani A, Braun A, Clark V, Jezzard P, Turner R. Cerebral organization for language in deaf and hearing subjects: biological constraints and effects of experience. *Proc Natl Acad Sci U S A*. 1998:95:922–929.
Newman MEJ, Girvan M. Finding and evaluating community structure in networks. *Phys Rev E*. 2004:69:026133.
Olulade OA, Koo DS, Lasasso CJ, Eden GF. Neuroanatomical profiles of deafness in the context of native language experience. *J Neurosci*. 2014:34:5613–5620.
Paillard J. Motor and representational framing of space. *Brain Sp*. 1991:182:147–162.
Pardoe HR, Abbott DF, Jackson GD. Sample size estimates for well-powered cross-sectional cortical thickness studies. *Hum Brain Mapp*. 2012:34:3000–3009.
Petitto LA, Zatorre RJ, Gauna K, Nikelski EJ, Dostie D, Evans AC. Speech-like cerebral activity in profoundly deaf people processing signed languages: implications for the neural basis of human language. *Proc Natl Acad Sci U S A*. 2000:97:13961–13966.
Pezzulo G, Zorzi M, Corbetta M. The secret life of predictive brains: what's spontaneous activity for? *Trends Cogn Sci*. 2021:25:730–743.
Power JD, Cohen AL, Nelson SM, Wig GS, Barnes KA, Church JA, Vogel AC, Laumann TO, Miezin FM, Schlaggar BL, et al. Functional network organization of the human brain. *Neuron*. 2011:72:665–678.
Pyers JE, Shusterman A, Senghas A, Spelke ES, Emmorey K. Evidence from an emerging sign language reveals that language supports spatial cognition. *Proc Natl Acad Sci U S A*. 2010:107:12116–12120.
Queralt A, Weerdesteyn V, Van Duijnhoven HJR, Castellote JM, Valls-solé J, Duysens J. The effects of an auditory startle on obstacle avoidance during walking. *J Physiol*. 2008:586:4453–4463.
Raichle ME, Macleod AM, Snyder AZ, Powers WJ, Gusnard DA, Shulman GL. A default mode of brain function. *Proc Natl Acad Sci U S A*. 2001:98:676–682.
Roberts JA, Perry A, Roberts G, Mitchell PB, Breakspear M. Consistency-based thresholding of the human connectome. *NeuroImage*. 2017:145:118–129.
Rubinov M, Sporns O. Complex network measures of brain connectivity: uses and interpretations. *NeuroImage*. 2010:52:1059–1069.
Sadaghiani S, Poline JB, Kleinschmidtc A, D'Esposito M. Ongoing dynamics in large-scale functional connectivity predict perception. *Proc Natl Acad Sci U S A*. 2015:112:8463–8468.
Sadato N, Yamada H, Okada T, Yoshida M, Hasegawa T, Matsuki KI, Yonekura Y, Itoh H. Age-dependent plasticity in the superior temporal sulcus in deaf humans: a functional MRI study. *BMC Neurosci*. 2004:5:1–6.
Sala-Llonch R, Peña-Gómez C, Arenaza-Urquijo EM, Vidal-Piñeiro D, Bargalló N, Junqué C, Bartrés-Faz D. Brain connectivity during resting state and subsequent working memory task predicts behavioural performance. *Cortex*. 2012:48:1187–1196.
Schultz DH, Cole MW. Higher intelligence is associated with less task-related brain network reconfiguration. *J Neurosci*. 2016:36: 8551–8561.
Schwarz AJ, McGonigle J. Negative edges and soft thresholding in complex network analysis of resting state functional connectivity data. *NeuroImage*. 2011:55:1132–1146.
Sha Z, Xia M, Lin Q, Cao M, Tang Y, Xu K, Song H, Wang Z, Wang F, Fox PT, et al. Meta-connectomic analysis reveals commonly disrupted functional architectures in network modules and connectors across brain disorders. *Cereb Cortex*. 2018:28:4179–4194.
Sharp A, Landry SP, Maheu M, Champoux F. Deafness alters the spatial mapping of touch. *PLoS One*. 2018:13:1–9.

Shiell MM, Champoux F, Zatorre RJ. Reorganization of auditory cortex in early-deaf people: functional connectivity and relationship to hearing aid use. *J Cogn Neurosci*. 2015:27:150–163.

Shine JM, Bissett PG, Bell PT, Koyejo O, Balsters JH, Gorgolewski KJ, Moodie CA, Poldrack RA. The dynamics of functional brain networks: integrated network states during cognitive task performance. *Neuron*. 2016:92:544–554.

Shulman GL, Fiez JA, Corbetta M, Buckner RL, Miezin FM, Raichle ME, Petersen SE. Common blood flow changes across visual tasks: II. Decreases in cerebral cortex. *J Cogn Neurosci*. 1997:9:648–663.

Simon M, Campbell E, Genest F, Maclean MW, Champoux F, Lepore F. The impact of early deafness on brain plasticity: a systematic review of the white and gray matter changes. *Front Neurosci*. 2020:14:206.

Smith SM, Fox PT, Miller KL, Glahn DC, Fox PM, Mackay CE, Filippini N, Watkins KE, Toro R, Laird AR, et al. Correspondence of the brain's functional architecture during activation and rest. *Proc Natl Acad Sci U S A*. 2009:106:13040–13045.

Smith KM, Mecoli MD, Altaye M, Komlos M, Maitra R, Eaton KP, Egelhoff JC, Holland SK. Morphometric differences in the Heschl's gyrus of hearing impaired and normal hearing infants. *Cereb Cortex*. 2011:21:991–998.

Smittenaar CR, MacSweeney M, Sereno MI, Schwarzkopf DS. Does congenital deafness affect the structural and functional architecture of primary visual cortex? *Open Neuroimaging J*. 2016:10: 1–19.

Sowell ER, Thompson PM, Leonard CM, Welcome SE, Kan E, Toga AW. Longitudinal mapping of cortical thickness and brain growth in normal children. *J Neurosci*. 2004:24:8223–8231.

Spadone S, Della Penna S, Sestieri C, Betti V, Tosoni A, Perrucci MG, Romani GL, Corbetta M. Dynamic reorganization of human resting-state networks during visuospatial attention. *Proc Natl Acad Sci U S A*. 2015:112:8112–8117.

Sulpizio S, Del Maschio N, Del Mauro G, Fedeli D, Abutalebi J. Bilingualism as a gradient measure modulates functional connectivity of language and control networks. *NeuroImage*. 2020:205:116306.

Sun Y, Dai Z, Li J, Collinson SL, Sim K. Modular-level alterations of structure–function coupling in schizophrenia connectome. *Hum Brain Mapp*. 2017:38:2008–2025.

Tamaki C, Maul K, Talian DS, Sparks S. Deaf individuals who report having good balance function present with significant vestibular deficits. *J Am Acad Audiol*. 2021:32:510–520.

Tavor I, Jones OP, Mars RB, Smith SM, Behrens TE, Jbabdi S. Task-free MRI predicts individual differences in brain activity during task performance. *Science*. 2016:80. 352:216–220.

Thompson GJ, Magnuson ME, Merritt MD, Schwarb H, Pan WJ, Mckinley A, Tripp LD, Schumacher EH, Keilholz SD. Short-time windows of correlation between large-scale functional brain networks predict vigilance intraindividually and interindividually. *Hum Brain Mapp*. 2013:34:3280–3298.

Twomey T, Waters D, Price CJ, Evans S, Macsweeney M. How auditory experience differentially influences the function of left and right superior temporal cortices. *J Neurosci*. 2017:37:9564–9573.

Tzourio-Mazoyer N, Landeau B, Papathanassiou D, Crivello F, Etard O, Delcroix N, Mazoyer B, Joliot M. Automated anatomical labeling of activations in SPM using a macroscopic anatomical parcellation of the MNI MRI single-subject brain. *NeuroImage*. 2002:15: 273–289.

van Den Heuvel MP, Fornito A. Brain networks in schizophrenia. *Neuropsychol Rev*. 2014:24:32–48.

Van Dijk R, Kappers AML, Postma A. Superior spatial touch: improved haptic orientation processing in deaf individuals. *Exp Brain Res*. 2013:230:283–289.

Van Essen DC. A tension-based theory of morphogenesis and compact wiring in the central nervous system. *Nature*. 1997:385(6614): 313–318.

van Wijk BCM, Stam CJ, Daffertshofer A. Comparing brain networks of different size and connectivity density using graph theory. *PLoS One*. 2010:5:e13701.

Vinh NX, Epps J, Bailey J. Information theoretic measures for clusterings comparison: variants, properties, normalization and correction for chance. *J Mach Learn Res*. 2010:11:2837–2854.

Weisz N, Wühle A, Monittola G, Demarchi G, Frey J, Popov T, Braun C. Prestimulus oscillatory power and connectivity patterns predispose conscious somatosensory perception. *Proc Natl Acad Sci U S A*. 2014:111:E417–E425.

Winfield DA. The postnatal development of synapses in the visual cortex of the cat and the effects of eyelid closure. *Brain Res*. 1981:206:166–171.

Winfield DA. The postnatal development of synapses in the different laminae of the visual cortex in the normal kitten and in kittens with eyelid suture. *Dev Brain Res*. 1983:9:155–169.

Yeo BTT, Krienen FM, Sepulcre J, Sabuncu MR, Lashkari D, Hollinshead M, Roffman JL, Smoller JW, Zöllei L, Polimeni JR, et al. The organization of the human cerebral cortex estimated by intrinsic functional connectivity. *J Neurophysiol*. 2011:106: 1125–1165.

Yoo K, Rosenberg MD, Noble S, Scheinost D, Constable RT, Chun MM. Multivariate approaches improve the reliability and validity of functional connectivity and prediction of individual behaviors. *NeuroImage*. 2019:197:212–223.

Yu X, Wang G, Gilmore A, Yee AX, Li X, Xu T, Smith SJ, Chen L, Zuo Y. Accelerated experience-dependent pruning of cortical synapses in Ephrin-A2 knockout mice. *Neuron*. 2013:80: 64–71.

Yusuf PA, Hubka P, Tillein J, Vinck M, Kral A. Deafness weakens interareal couplings in the auditory cortex. *Front Neurosci*. 2021:14:1476.

Yusuf PA, Lamuri A, Hubka P, Tillein J, Vinck M, Kral A. Deficient recurrent cortical processing in congenital deafness. *Front Syst Neurosci*. 2022:16:806142.

Zaehle T, Jordan K, Wüstenberg T, Baudewig J, Dechent P, Mast FW. The neural basis of the egocentric and allocentric spatial frame of reference. *Brain Res*. 2007:1137:92–103.

Zhang M, Tan X, Shen L, Wang A, Geng S, Chen Q. Interaction between allocentric and egocentric reference frames in deaf and hearing populations. *Neuropsychologia*. 2014:54:68–76.